

# Differential Cross Section for Higgs Boson Production Including All-Orders Soft Gluon Resummation

Edmond L. Berger<sup>1,\*</sup> and Jianwei Qiu<sup>2,†</sup>

<sup>1</sup>*High Energy Physics Division, Argonne National Laboratory, Argonne, IL 60439*

<sup>2</sup>*Department of Physics and Astronomy,  
Iowa State University, Ames, IA 50011*

(Dated: February 8, 2020)

## Abstract

The transverse momentum  $Q_T$  distribution is computed for inclusive Higgs boson production at the energy of the CERN Large Hadron Collider. We focus on the dominant gluon-gluon subprocess in perturbative quantum chromodynamics and incorporate contributions from the quark-gluon and quark-antiquark channels. Using an impact-parameter  $b$ -space formalism, we include all-orders resummation of large logarithms associated with emission of soft gluons. Our resummed results merge smoothly at large  $Q_T$  with the fixed-order expectations in perturbative quantum chromodynamics, as they should, with no need for a matching procedure. They show a high degree of stability with respect to variation of parameters associated with the non-perturbative input at low  $Q_T$ . We provide distributions  $d\sigma/dy dQ_T$  for Higgs boson masses from  $M_Z$  to 200 GeV. The average transverse momentum at zero rapidity  $y$  grows approximately linearly with mass of the Higgs boson over the range  $M_Z < m_h < 200$  GeV,  $\langle Q_T \rangle \simeq 0.21m_h + 22$  GeV. We provide analogous results for  $Z$  boson production, for which we compute  $\langle Q_T \rangle \simeq 25$  GeV. The harder transverse momentum distribution for the Higgs boson arises because there is more soft gluon radiation in Higgs boson production than in  $Z$  production.

---

\*e-mail: berger@anl.gov

†e-mail: jwq@iastate.edu

## I. INTRODUCTION

The breaking of electroweak symmetry in the standard model (SM) of elementary particle interactions is achieved through the Higgs mechanism. In the simplest realization, a complex Higgs doublet is introduced, and a single neutral CP-even Higgs boson is predicted. Two Higgs doublets are expected at low energies in supersymmetric extensions of the standard model. The lightest neutral CP-even Higgs particle  $h$  resembles the SM Higgs boson in most regions of parameter space of broken supersymmetry [1]. Direct experimental searches at the CERN Large Electron Positron Collider (LEP) based on the presumption of significant decay branching ratio into bottom ( $b$ ) quarks place the mass of a SM-like Higgs state above approximately 115 GeV [2]. An alternative analysis, based on the assumption of Higgs boson decay into hadronic jets, without  $b$ -tagging, provides a bound of about 113 GeV [3]. A good theoretical description of electroweak data [4] in the framework of the SM requires the Higgs boson to be lighter than about 200 GeV [2]. Within the minimal supersymmetric standard model (MSSM), the upper bound on the mass of the lightest Higgs state is roughly 135 GeV [5]. The search for the Higgs boson is a central motivation for the experimental programs at the Fermilab Tevatron and the CERN Large Hadron Collider (LHC), with detection techniques guided by theoretical expectations about its production dynamics and decay properties.

A Higgs boson resembling one anticipated by the SM is expected to be discovered at the LHC through various partonic production processes and decays to SM particles [6, 7]. These include

- $gg \rightarrow hX$ , with  $h \rightarrow \gamma\gamma$ ,  $h \rightarrow W^+W^-$ , or  $h \rightarrow ZZ$  ;
- $gg \rightarrow t\bar{t}hX$ , with  $h \rightarrow b\bar{b}$  or  $h \rightarrow \gamma\gamma$  ; and
- $W^+W^-(ZZ) \rightarrow hX$ , with  $h \rightarrow W^+W^-$ ,  $h \rightarrow \gamma\gamma$ , or  $h \rightarrow \tau^+\tau^-$ .

The fully inclusive gluon-gluon fusion subprocess [8, 9]  $gg \rightarrow hX$  is the dominant mechanism of production. In this process, production occurs through triangle loops of colored (s)particles that couple to the Higgs boson and to gluons. In the SM, the most relevant contribution is from a loop of top ( $t$ ) quarks, with a small contribution from bottom quark loops. In supersymmetric theories, the bottom quark loop contribution can be important for small  $m_A$  and large values of  $\tan\beta$ , where  $m_A$  is the mass of the pseudo-scalar Higgs

boson and  $\tan\beta$  is the ratio of Higgs vacuum expectation values. In the MSSM, loops of bottom squarks may make an important contribution if the mass of the bottom squark is light enough [10].

Semi-inclusive production of the Higgs boson in association with top quarks,  $gg \rightarrow t\bar{t}hX$ , has a relatively low rate because of the large masses in the final state. The semi-inclusive weak boson fusion modes [11]  $W^+W^-(ZZ) \rightarrow hX$  require identification of (forward) “trigger” jets from subprocesses such as  $qq \rightarrow qqWW \rightarrow qqhX$ . Searches at the Tevatron rely on associated production of the Higgs boson with weak bosons,  $W$  and  $Z$ , and the decay mode  $h \rightarrow b\bar{b}$  [12].

For masses  $m_h$  of the Higgs boson up to about 150 GeV, the SM Higgs boson produced in the gluon fusion process should be discovered at the LHC in the rare di-photon decay mode  $h \rightarrow \gamma\gamma$  [6, 7]. Once data are in hand, the immense  $\gamma\gamma$  background from various sources can be determined from the data by a measurement of the di-photon invariant mass distribution  $d\sigma/dM_{\gamma\gamma}$  on both sides of the Higgs resonance. Beforehand, precise theoretical calculations of the expected differential cross sections for production of the signal and backgrounds [13, 14, 15] are important for quantitative evaluation of the required measurement accuracies and detector performance. Good estimations of the expected transverse momentum distributions can suggest selections in this variable that should improve background rejection. In this paper, we concentrate on behavior of the Higgs boson transverse momentum distribution in the region of small and intermediate values of  $Q_T$ .

Above  $W^+W^-$  threshold but below  $Z$ -pair threshold, the decay mode  $h \rightarrow W^+W^-$  has a branching ratio approaching 100%. Because there are missing neutrinos in the leptonic decay modes of the  $W$ ’s, the invariant mass distribution of the Higgs boson cannot be reconstructed directly, but the transverse mass spectrum of the  $(\ell^+ \ell^- \cancel{E}_T)$  system can be measured. This distribution is expected to be broad, and straightforward sideband determinations of the background are not possible. However, measurements of the backgrounds in regions in which the signal is expected to be absent can then be extrapolated into the expected signal region provided that good predictions are available of differential cross sections.

In the SM, the coupling of gluons to the Higgs boson through the top quark loop is simplified in the limit of large top quark mass  $m_t$ . In this limit, the relevant Feynman diagrams are obtained from an effective Lagrangian [16]. For inclusive production integrated over all transverse momentum, the next-to-leading order contributions in perturbative quantum

chromodynamics (QCD) are reported in Ref. [17]. The  $m_t \rightarrow \infty$  approximation is valid to an accuracy of  $\sim 5\%$  for  $m_h \leq 2m_t$ . Within this approach, the total cross section for  $gg \rightarrow hX$ , is known to next-to-next-to-leading order accuracy [18].

Computations of the transverse momentum distribution for Higgs boson production at leading order in perturbative QCD [19] show that the large  $m_t$  approximation serves well when the Higgs boson mass  $m_h$  is less than twice the top quark mass and the Higgs boson transverse momentum  $Q_T$  is less than  $m_t$ . The next-to-leading order contributions to the transverse momentum distribution are computed with numerical integration methods in Ref. [20]. The doubly-differential cross section in rapidity and transverse momentum of the Higgs boson is computed analytically at next-to-leading order in Refs. [21] and [22].

When the transverse momentum  $Q_T$  is comparable to the mass  $m_h$  of the Higgs boson, there is only one hard momentum scale in the perturbative expansion of the cross section as a function of the strong coupling  $\alpha_s$ , and fixed-order computations in perturbative QCD are expected to be applicable. However, in the region  $Q_T \ll m_h$ , where the cross section is greatest, the coefficients of the expansion in  $\alpha_s$  depend functionally on logarithms of the ratio of the two quantities,  $m_h$  and  $Q_T$ . A well-studied case is the cross section for gauge boson (W, Z, or virtual photon) production in hadronic collisions, at measured transverse momentum. The logarithmic term is  $(\alpha_s/\pi) \ln^2(Q^2/Q_T^2)$  where  $Q$  is the mass of the boson and  $Q_T$  its transverse momentum. For Higgs boson production at  $m_h = 125$  GeV, the peak of the transverse momentum distribution is expected to occur near  $Q_T = 14$  GeV at LHC energies, as is shown in this paper. Correspondingly,  $\ln^2(m_h^2/Q_T^2) \sim 19$  and  $(\alpha_s(\mu)/\pi) \ln^2(m_h^2/Q_T^2) \sim 0.7$  if  $\mu = m_h$  or  $\sim 1.1$  if  $\mu = Q_T$ . In either case, the relevant expansion parameter in the perturbative series is close to 1, meaning that higher order contributions in perturbation theory are not suppressed. When  $Q_T \ll m_h$ , straightforward perturbation theory is inapplicable. Indeed, even at leading order in  $\alpha_s$ , the computed cross section  $d\sigma/dQ_T^2$  includes a term proportional to  $(\alpha_s/Q_T^2) \ln(m_h^2/Q_T^2)$ . This divergence as  $Q_T \rightarrow 0$  is obviously unphysical.

All-orders resummation is the established method for mastering the large logarithmic coefficients of the expansion in  $\alpha_s$  and for obtaining well-behaved cross sections at intermediate and small  $Q_T$  [23, 24, 25]. It is a reorganization of the perturbative expansion that brings the large logarithmic terms under systematic control, providing finite predictions for the  $Q_T$  dependence that are different from those at fixed order. Resummation overcomes the limitations of fixed-order calculations but still incorporates all the information that these

calculations offer.

Resummation may be carried out in either  $Q_T$  [25] or impact parameter ( $b$ ) space, which is the Fourier conjugate of  $Q_T$  space. All else being equal, the  $b$  space approach has the advantage that transverse momentum conservation is explicit. Using renormalization group techniques, Collins, Soper, and Sterman (CSS) [24] devised a  $b$  space resummation formalism that resums all logarithmic terms as singular as  $(1/Q_T^2) \ln^n(Q^2/Q_T^2)$  when  $Q_T \rightarrow 0$ . This formalism has been used widely for computations of the transverse momentum distributions of vector bosons in hadron reactions [26, 27, 28, 29, 30, 31, 32, 33, 34], Higgs bosons [35, 36, 37, 38, 39], and other processes [14, 40].

In many of these applications of the CSS formalism, two difficulties significantly limit its predictive power in the region of small and intermediate values of  $Q_T$ . The first of these is the ambiguity, if not discontinuity in  $Q_T$ , associated with the “matching” of the resummed and fixed-order calculations in a region of  $Q_T$  below which the resummed form is used, and above which a fixed-order expression is used. The second difficulty is associated with the quantitative importance of assumed forms for non-perturbative functions that, in many implementations, dominate the  $Q_T$  distribution in the region of very small  $Q_T$  and affect even the  $Q_T$  distribution at large  $Q_T$ . In recent papers [32], Qiu and Zhang demonstrate that both of these drawbacks can be overcome. By using an integral form for the oscillatory Bessel function in the Fourier transform, they show that the  $b$ -space resummation procedure produces smooth distributions for all  $Q_T < Q$ , obviating the need for a matching prescription. Second, to substantially reduce the influence of phenomenological non-perturbative functions, they derive a new functional expression that extrapolates the perturbatively calculated  $b$ -space resummation expression from the region of small  $b$ , where it is valid, to the region of large  $b$  where non-perturbative input is needed. Their analysis shows that perturbation theory itself indicates the form of the required non-perturbative power corrections. They also demonstrate that the predictive power of resummation improves considerably with total center-of-mass collision energy  $\sqrt{S}$ . In this paper, we further develop the methodology of Qiu and Zhang and use it to study the production of Higgs bosons.

In Sec. II, we review the pertinent aspects of the  $b$ -space resummation formalism, with particular emphasis on Higgs boson production. Working at next-to-leading-logarithm (NLL) accuracy, we resum both leading and next-to-leading logarithmic terms associated with soft gluon emission to all orders in  $\alpha_s$ . At LHC energies, the typical values of the

incident parton momentum fractions  $x_A \sim x_B \sim m_h/\sqrt{S} \sim 0.009$  (for  $m_h = 125$  GeV) are small, and the gluon distribution evolves steeply at small  $x$ . Consequently, the saddle point in  $b$  of the Fourier transform from  $b$ -space to  $Q_T$  space is well into the region of perturbative validity. Resummed perturbation theory is valid at small  $b$ , just as perturbative QCD is valid at large  $Q_T$ . However, the Fourier transform from  $b$ -space to  $Q_T$ -space requires specification of the  $b$ -space distribution for all  $b$ . In Sec. III, we show that the region of large  $b$  becomes progressively less important quantitatively as  $\sqrt{S}$  increases. The  $Q_T$  distribution at LHC energies is entirely insensitive to the functional form we employ for the non-perturbative input at large  $b$ , so long as the form used for this extrapolation does not modify the  $b$ -space distribution at small  $b$ . In Sec. III.B, we discuss the extrapolation from the region of small  $b$  to the region of large  $b$ , and we specify the form we use for the non-perturbative functions at large  $b$ . We discuss why other approaches in the literature may introduce inappropriate dependence on  $\sqrt{S}$ . We provide analytic expressions for the fixed-order perturbative subprocesses in Sec. IV. We employ expressions for the parton-level hard-scattering functions valid through first-order in  $\alpha_s$ , including contributions from the glue-gluon, quark-gluon, and quark-antiquark incident partonic subprocesses.

Numerical predictions are presented in Sec. V. We show the doubly differential cross section  $d\sigma/dy dQ_T$  as a function of  $Q_T$  at fixed rapidity  $y = 0$ , and the  $Q_T$  distributions for rapidity integrated over the interval  $|y| < 2.4$ . We present results for four choices of mass of the Higgs boson, values that span the range of present interest in the SM, from  $m_h = M_Z = 91.187$  GeV to  $m_h = 200$  GeV. To illustrate interesting differences, we also show our results for  $Z$  boson production at the same energy. Our resummed results make a smooth transition to the fixed-order perturbative results near or just above  $Q_T = Q$ , for all  $Q$ , without need of a supplementary matching procedure. Our implementation of the resummation formalism works smoothly throughout the  $Q_T$  region even for the distributions differential in rapidity,  $d\sigma/dy dQ_T$ . Two points are evident in the comparison of  $Z$  boson and Higgs boson production, with  $m_h = M_Z$ . The peak in the  $Q_T$  distribution occurs at a smaller value of  $Q_T$  for  $Z$  production (4.8 GeV *vs.* 11.6 GeV) and the distribution is narrower for  $Z$  production. The larger QCD color factors produce more gluonic showering in the glue-gluon scattering subprocess that dominates inclusive Higgs boson production than in the fermionic subprocesses relevant for  $Z$  production. After all-orders resummation, the enhanced showering suppresses the large- $b$  (small  $Q_T$ ) region more effectively for Higgs

boson production. We compare the predicted  $Q_T$  distributions for Higgs boson production at different masses. The peak of the distribution shifts to greater  $Q_T$  as  $m_h$  grows, in approximately linear fashion, and the distribution broadens somewhat. The mean value  $\langle Q_T \rangle$  grows from about 41 GeV at  $m_h = M_Z$  to about 65 GeV at  $m_h = 200$  GeV, and the root-mean-square grows from about 65 GeV to about 98 GeV. For  $Z$  production, we find  $\langle Q_T \rangle = 25$  GeV and  $\langle Q_T^2 \rangle^{1/2} = 38$  GeV. The harder  $Q_T$  spectrum suggests that the signal to background ratio can be enhanced if Higgs bosons are selected with large  $Q_T$ .

Choices of variable parameters are made in obtaining our results, and we examine the sensitivity of the results to these choices, including the renormalization/factorization scale  $\mu$  and the non-perturbative input. Scale dependence is the most important source of uncertainty. It can shift the position of the peak by about 1.5 GeV, with corresponding changes in the normalization of the distribution above and below the position of the peak. The value of  $d\sigma/dy dQ_T$  at the peak position is shifted by 4 to 5%. Changes in the parameters of the non-perturbative input produce effects that at most 1 to 2% depending on the size of the power corrections we introduce. In the formulation we use to describe the non-perturbative region, there is essentially no effect on the behavior of differential cross section at large  $Q_T$ . In comparison with prior work, we note that the locations of the maxima in the distributions  $d\sigma/dy dQ_T$  occur at somewhat larger values of  $Q_T$  in our case, and the distributions themselves differ as a function of  $Q_T$  above the location of the maximum. The differences arise from the different treatment of the non-perturbative input. In our approach, the assumed parametrization of non-perturbative effects has the desirable property that it does not affect the physics in the perturbative region  $b < 0.5$  GeV.

Conclusions are summarized in Sec. VI.

## II. ALL-ORDERS RESUMMED $Q_T$ DISTRIBUTION

We consider the inclusive hadronic reaction in which a color neutral heavy boson of invariant mass  $Q$  is produced:

$$A(P_A) + B(P_B) \rightarrow C(Q) + X, \quad (1)$$

with  $C = \gamma^*, W^\pm, Z$ , or a Higgs boson in the limit in which the top quark mass  $m_t \gg Q/2$ . The square of the total center-of-mass energy of the collision is  $S$ . At the LHC,  $\sqrt{S} = 14$  TeV.

In the CSS resummation formalism, the differential cross section is written as the sum

$$\frac{d\sigma_{AB \rightarrow CX}}{dQ^2 dy dQ_T^2} = \frac{d\sigma_{AB \rightarrow CX}^{(\text{resum})}}{dQ^2 dy dQ_T^2} + \frac{d\sigma_{AB \rightarrow CX}^{(\text{Y})}}{dQ^2 dy dQ_T^2}. \quad (2)$$

The all-orders resummed term is a Fourier transform from  $b$ -space

$$\begin{aligned} \frac{d\sigma_{AB \rightarrow CX}^{(\text{resum})}}{dQ^2 dy dQ_T^2} &= \frac{1}{(2\pi)^2} \int d^2b e^{i\vec{Q}_T \cdot \vec{b}} W_{AB \rightarrow CX}(b, Q, x_A, x_B) \\ &= \int \frac{db}{2\pi} J_0(Q_T b) b W_{AB \rightarrow CX}(b, Q, x_A, x_B), \end{aligned} \quad (3)$$

where  $J_0$  is a Bessel function. The function  $W_{AB \rightarrow CX}(b, Q, x_A, x_B)$  resums to all orders in QCD perturbation theory the singular terms that would otherwise behave as  $\delta^2(Q_T)$  and  $(1/Q_T^2) \ln^m(Q^2/Q_T^2)$ , for all  $m \geq 0$ . The variables  $x_A$  and  $x_B$  are light-cone momentum fractions carried by the incident partons from hadrons  $A$  and  $B$ :

$$x_A = \frac{Q}{\sqrt{S}} e^y \quad \text{and} \quad x_B = \frac{Q}{\sqrt{S}} e^{-y}, \quad (4)$$

and  $y$  is the rapidity of the heavy boson. The variables  $x_A$  and  $x_B$  do not depend on  $Q_T$ .

Resummation treats only the parts of the fixed-order QCD expression that are at least as singular as  $Q_T^{-2}$  in the limit  $Q_T \rightarrow 0$ . The remainder, including possible less singular pieces of the fixed-order perturbative contribution, is defined as the difference of the cross section computed at fixed order  $n$  in perturbation theory and its  $Q_T \ll Q$  asymptote that is at least as singular as  $Q_T^{-2}$ .

$$\frac{d\sigma_{AB \rightarrow CX}^{(\text{Y})}}{dQ^2 dy dQ_T^2} = \frac{d\sigma_{AB \rightarrow CX}^{(\text{pert})}}{dQ^2 dy dQ_T^2} - \frac{d\sigma_{AB \rightarrow CX}^{(\text{asym})}}{dQ^2 dy dQ_T^2}. \quad (5)$$

This remainder is not significant quantitatively at modest  $Q_T$ , since the dominant singularities of the two terms on the right-hand-side cancel in the region  $Q_T \rightarrow 0$ . However, the difference becomes important when  $Q_T \sim Q$ . Explicit expressions for the fixed-order remainder terms are presented in Sec. IV.

We may factor out the lowest order partonic cross section and rewrite the function  $W_{AB \rightarrow CX}(b, Q, x_A, x_B)$  that appears in the integrand of Eq. (3) as

$$W_{AB \rightarrow CX}(b, Q, x_A, x_B) = \sum_{ij} W_{ij}(b, Q, x_A, x_B) \sigma_{ij \rightarrow CX}^{(0)}(Q). \quad (6)$$



Here,  $\sigma_{ij \rightarrow CX}^{(0)}(Q)$  is the lowest order cross section for a pair of partons of flavor  $i$  and  $j$  to produce a heavy boson of invariant mass  $Q$ . Because the heavy boson is color neutral, the parton flavors  $ij$  can be either the quark-antiquark or the gluon-gluon combination.

### A. Higgs boson production

Specializing to Higgs boson  $h$  production in gluon-gluon fusion (and using  $m_h$  and  $Q$  interchangeably for the Higgs boson mass in the remainder of this paper), we write

$$W_{AB \rightarrow hX}(b, Q, x_A, x_B) = W_{gg}(b, Q, x_A, x_B) \sigma_{gg \rightarrow hX}^{(0)}(Q). \quad (7)$$

In the effective Lagrangian approximation [16, 17] where we keep only the contribution from the top quark loop, the lowest order partonic cross section for  $gg \rightarrow hX$  is

$$\sigma_{gg \rightarrow hX}^{(0)}(Q) = \sigma_0 \frac{\pi}{S} m_h^2 \delta(Q^2 - m_h^2), \quad (8)$$

with

$$\sigma_0 = \left( \sqrt{2} G_F \right) \frac{\alpha_s^2(\mu_r)}{576\pi}. \quad (9)$$

In this expression,  $G_F$  is the Fermi constant, and  $\mu_r$  denotes a renormalization scale. We note that  $\sigma_0$  is formally of second order in the strong coupling strength. However, we *define*  $\sigma_0$  be the effective 0'th order cross section and focus on the influence of yet higher order contributions. If we were to include contributions other than from top quarks in the loop, whether from bottom quarks or bottom squarks, we could easily replace  $\sigma_0$  by a different expression. This inclusion would change the overall normalization of our predictions. For on-mass-shell gluons, QCD corrections to the  $ggh$  effective vertex are known to order  $\alpha_s^2$  [41] and likewise could be incorporated in a change in the numerical value of the effective  $\sigma_0$ .

For comparison with Eq. (8), we also present the expression for the lowest order massive lepton-pair Drell-Yan cross section:

$$\sigma_{q\bar{q} \rightarrow \ell^+ \ell^- X}^{(0)}(Q) = e_q^2 \frac{4\pi^2 \alpha_{em}^2}{9SQ^2}. \quad (10)$$

## B. Evolution equation for resummation

Resummation of the large logarithmic terms is achieved in the CSS formalism through a solution of the evolution equation

$$\frac{\partial}{\partial \ln Q^2} W_{gg}(b, Q, x_A, x_B) = \left[ K_g(b\mu, \alpha_s(\mu)) + G_g\left(\frac{Q}{\mu}, \alpha_s(\mu)\right) \right] W_{gg}(b, Q, x_A, x_B), \quad (11)$$

where the subscripts  $g$  and  $gg$  indicate the gluonic process. There are two physical momentum variables in this expression,  $Q$  and  $1/b$ , as well dependence on the scale variable  $\mu$  that, in principle, could take on values from of order  $1/b$  to of order  $Q$ . However, the  $\mu$  dependence of  $K_g$  and  $G_g$  is determined by renormalization group equations (RGE's),

$$\frac{\partial}{\partial \ln \mu^2} K_g(b\mu, \alpha_s(\mu)) = -\frac{1}{2} \gamma_g(\alpha_s(\mu)), \quad (12)$$

$$\frac{\partial}{\partial \ln \mu^2} G_g\left(\frac{Q}{\mu}, \alpha_s(\mu)\right) = \frac{1}{2} \gamma_g(\alpha_s(\mu)). \quad (13)$$

The RGE's for  $K_g$  and  $G_g$  ensure that  $d/d \ln(\mu^2)[W_{gg}(b, Q, x_A, x_B)] = 0$  perturbatively, an expression that is consistent with the fact that  $W_{gg}$  is effectively a physical observable. The coefficients  $\gamma_g^{(n)}$  in an expansion of the anomalous dimension  $\gamma_g(\alpha_s(\mu)) = \sum_{n=1} \gamma_g^{(n)}(\alpha_s(\mu)/\pi)^n$  are calculable perturbatively.

The RGE's for  $K_g$  and  $G_g$  may be integrated over  $\ln(\mu^2)$  from  $\ln(C_1^2/b^2)$  to  $\ln(\mu^2)$ , and from  $\ln(\mu^2)$  to  $\ln(C_2^2 Q^2)$ , respectively, where  $C_1$  and  $C_2$  are integration constants. The values of  $C_1$  and  $C_2$  are somewhat arbitrary. Following CSS, we select  $C_1 = c = 2e^{-\gamma_E} = \mathcal{O}(1)$ , where Euler's constant  $\gamma_E \approx 0.577$ , and  $C_2 = 1$ . After the integrations, one derives

$$K_g(b\mu, \alpha_s(\mu)) + G_g(Q/\mu, \alpha_s(\mu)) = - \int_{c^2/b^2}^{Q^2} \frac{d\bar{\mu}^2}{\bar{\mu}^2} A_g(\alpha_s(\bar{\mu})) - B_g(\alpha_s(Q)), \quad (14)$$

where  $A_g$  is a function of  $\gamma_g(\alpha_s(\bar{\mu}))$  and  $K_g(c, \alpha_s(\bar{\mu}))$  while  $B_g$  depends on both  $K_g(c, \alpha_s(Q))$  and  $G_g(1, \alpha_s(Q))$ . The choice of  $C_1 = c = 2e^{-\gamma_E}$  and  $C_2 = 1$  has the virtue of removing logarithmic dependence on these parameters from the functions  $A_g$  and  $B_g$ .

The functions  $A_g$  and  $B_g$  are free of logarithmic dependence and have well-behaved perturbative expansions

$$A_g(\alpha_s(\bar{\mu})) = \sum_{n=1} A_g^{(n)} \left( \frac{\alpha_s(\bar{\mu})}{\pi} \right)^n \quad \text{and} \quad B_g(\alpha_s(\bar{\mu})) = \sum_{n=1} B_g^{(n)} \left( \frac{\alpha_s(\bar{\mu})}{\pi} \right)^n. \quad (15)$$

The first two coefficients in the expansions for  $A$  and  $B$  are known [37, 38, 39]. For the choices  $C_1 = c = 2e^{-\gamma_E}$  and  $C_2 = 1$ , these are

$$\begin{aligned}
A_g^{(1)} &= C_A, \\
A_g^{(2)} &= \frac{C_A}{2} \left[ C_A \left( \frac{67}{18} - \frac{\pi^2}{6} \right) - \frac{5}{9} n_F \right], \\
B_g^{(1)} &= -\frac{11C_A - 2n_F}{6}, \\
B_g^{(2)} &= C_A^2 \left( \frac{23}{24} + \frac{11}{18} \pi^2 - \frac{3}{2} \zeta(3) \right) + \frac{1}{2} C_F n_F \\
&\quad - C_A n_F \left( \frac{1}{12} + \frac{\pi^2}{9} \right) - \frac{11}{8} C_A C_F.
\end{aligned} \tag{16}$$

Here,  $\zeta(3)$  is the third Riemann function,  $n_F = 5$  is the number of active quark flavors, and

$$C_A = N_c = 3, \quad \text{and} \quad C_F = \frac{N_c^2 - 1}{2N_c} = \frac{4}{3} \tag{17}$$

for SU(3) color. The corresponding fermionic coefficients  $A_q^{(i)}$  and  $B_q^{(i)}$ , with  $i = 1, 2$  are found in Refs. [24, 26]. The coefficient  $A_q^{(3)}$  is available in numerical form [42].

The solution of the linear evolution Eq. (11) may be written in the form

$$W_{gg}(b, Q, x_A, x_B) = e^{-S_g(b, Q)} W_{gg}(b, \frac{c}{b}, x_A, x_B). \tag{18}$$

The function  $W_{gg}(b, c/b, x_A, x_B)$  depends on only one momentum variable,  $1/b$ , and it can be computed in perturbation theory as long as  $1/b$  is large enough. All large logarithmic terms from  $\ln(c^2/b^2)$  to  $\ln(Q^2)$  are resummed to all orders in  $\alpha_s$  in the exponential factor, with

$$S_g(b, Q) = \int_{c^2/b^2}^{Q^2} \frac{d\bar{\mu}^2}{\bar{\mu}^2} \left[ \ln \left( \frac{Q^2}{\bar{\mu}^2} \right) A_g(\alpha_s(\bar{\mu})) + B_g(\alpha_s(\bar{\mu})) \right]. \tag{19}$$

The appearance of  $(c/b)^2$  as the lower limit of integration serves to cut off the non-perturbative region of small  $Q_T$ .

The function  $W_{gg}(b, c/b, x_A, x_B)$  may be written in factored form as [24, 25]

$$W_{gg}(b, \frac{c}{b}, x_A, x_B) = f_{g/A}(x_A, \mu, \frac{c}{b}) f_{g/B}(x_B, \mu, \frac{c}{b}), \tag{20}$$

where  $f_{g/A}$  and  $f_{g/B}$  are modified gluon parton distributions

$$f_{g/A}(x_A, \mu, \frac{c}{b}) = \sum_a \int_{x_A}^1 \frac{d\xi}{\xi} \phi_{a/A}(\xi, \mu) C_{a \rightarrow g} \left( \frac{x_A}{\xi}, \mu, \frac{c}{b} \right). \tag{21}$$

Here we see the normal appearance of a factorization scale  $\mu$ , the scale of factorization between short-distance hard-scattering and the long-distance physics represented by the parton densities. The sum in Eq. (21) runs over all parton types, and  $\phi_{a/A}(\xi, \mu)$  is the usual momentum ( $\xi$ ) distribution of parton  $a$  from hadron  $A$  at the scale  $\mu$ . The short-distance coefficient functions are expanded in a perturbative series as

$$C_{a \rightarrow b} \left( z, \mu, \frac{c}{b} \right) = \sum_{n=0} C_{a \rightarrow b}^{(n)}(z, \mu, b) \left( \frac{\alpha_s(\mu)}{\pi} \right)^n. \quad (22)$$

The first two coefficients in the expansion of  $C$  are published [37, 38, 39]:

$$\begin{aligned} C_{g \rightarrow g}^{(0)} \left( z, \mu, \frac{c}{b} \right) &= \delta(1 - z), \\ C_{i \rightarrow g}^{(0)} \left( z, \mu, \frac{c}{b} \right) &= 0, \\ C_{g \rightarrow g}^{(1)} \left( z, \mu, \frac{c}{b} \right) &= \delta(1 - z) \left[ C_A \left( \frac{\pi^2}{4} + \frac{5}{4} \right) - \frac{3}{4} C_F \right] \\ &\quad - P_{g \rightarrow g}(z) \ln \left( \frac{\mu b}{c} \right), \\ C_{i \rightarrow g}^{(1)} \left( z, \mu, c/b \right) &= \frac{1}{2} C_F z - P_{i \rightarrow g}(z) \ln \left( \frac{\mu b}{c} \right). \end{aligned} \quad (23)$$

Here  $i$  represents a quark or antiquark flavor, and  $P_{g \rightarrow g}(z)$  and  $P_{i \rightarrow g}(z)$  are leading order parton-to-parton splitting functions,

$$\begin{aligned} P_{g \rightarrow g}(z) &= 2C_A \left[ \frac{z}{(1-z)_+} + \frac{(1-z)}{z} + z(1-z) \right] + \frac{11C_A - 2n_F}{6} \delta(1-z), \\ P_{i \rightarrow g}(z) &= C_F \left[ \frac{1 + (1-z)^2}{z} \right]. \end{aligned} \quad (24)$$

There is only one momentum scale,  $1/b$ , involved in the hard-scattering function  $W_{gg}(b, c/b, x_A, x_B)$ . Therefore, it is natural to choose  $\mu = c/b$  in the modified parton densities  $f_g(x, \mu, c/b)$  in order to remove the logarithmic terms in Eq. (23). However, this choice is not required. In principle,  $\mu$  may be any large momentum scale, *e.g.*,  $Q$ . This freedom is equivalent to the statement  $d/d \ln(\mu^2)[W_{gg}(b, c/b, x_A, x_B)] = 0$  order-by-order in powers of  $\alpha_s$ ; or,  $d/d \ln \mu^2 f_g(x_A, \mu, c/b) = 0$  order-by-order in  $\alpha_s$  for  $f_g$  defined in Eq. (21). The  $\mu$ -dependence in  $C_{a \rightarrow g}$  is compensated by the  $\mu$ -dependence in the parton densities. To order  $\alpha_s$ , we derive

$$\frac{d}{d \ln \mu^2} f_g(x, \mu, \frac{c}{b}) = \sum_a \int_x^1 \frac{d\xi}{\xi} \left[ \frac{d}{d \ln \mu^2} \phi_a(\xi, \mu) \right] C_{a \rightarrow g}^{(0)} \left( \frac{x}{\xi}, \mu, \frac{c}{b} \right)$$

$$\begin{aligned}
& + \sum_a \int_x^1 \frac{d\xi}{\xi} \phi_a(\xi, \mu) \left[ \frac{d}{d \ln \mu^2} C_{a \rightarrow g}^{(1)}\left(\frac{x}{\xi}, \mu, \frac{c}{b}\right) \right] \\
& = \sum_a \int_x^1 \frac{d\xi}{\xi} \left[ \frac{d}{d \ln \mu^2} \phi_a(\xi, \mu) \right] \delta_{ag} \delta\left(1 - \frac{x}{\xi}\right) \\
& + \sum_a \int_x^1 \frac{d\xi}{\xi} \phi_{a/A}(\xi, \mu) \left[ -\frac{\alpha_s}{2\pi} P_{a \rightarrow g}\left(\frac{x}{\xi}\right) \right] \\
& = 0.
\end{aligned} \tag{25}$$

The last equality follows because both terms on the right-hand-side equal  $(d/d \ln \mu^2) \phi_g(x, \mu)$ .

For simplicity, we elect to drop the subscript  $AB \rightarrow hX$  for the  $b$ -space distribution  $W_{AB \rightarrow hX}(b, Q, x_A, x_B)$ . In its region of validity at small  $b$  it takes the factored form

$$W^{\text{pert}}(b, Q, x_A, x_B) = \sigma_{gg \rightarrow hX}^{(0)} \sum_{a,b} \left[ \phi_{a/A} \otimes C_{a \rightarrow g} \right] \otimes \left[ \phi_{b/B} \otimes C_{b \rightarrow g} \right] \times e^{-S(b, Q)}, \tag{26}$$

where  $\otimes$  represents a convolution over parton momentum fractions. Since leading-twist perturbative QCD and normal parton densities are valid only for a hard scale  $\mu > \mu_0 \sim 1$  to 2 GeV, we expect naively that  $W^{\text{pert}}(b, Q, x_A, x_B)$  will be reliable for  $b < 1/\mu_0 \sim 1.0 \text{ GeV}^{-1}$ .

To perform the Fourier transform in Eq. (3), we require an expression for  $W(b, Q, x_A, x_B)$  that can be used over the entire range of integration in  $b$ . To the extent that the region of large  $b$  is important in the integrand, we must devise a functional form for  $W(b, Q, x_A, x_B)$  that extends into the region of large  $b$ , a topic addressed quantitatively in Sec. III. B.

In the CSS formalism, the coefficient functions  $C_{i \rightarrow j}$  and the Sudakov form factor  $S(b, Q)$  are process dependent. As discussed recently in Ref. [43], it is possible to reorganize the perturbatively calculated coefficient functions  $C_{i \rightarrow j}$  and the Sudakov form factor  $S(b, Q)$  to make them universal. This universality is achieved if an all orders process-dependent hard part  $H_{gg}(\alpha_s(Q))$  is introduced into Eq. (26),

$$W_H^{\text{pert}}(b, Q, x_A, x_B) = \sigma_{gg \rightarrow hX}^{(0)} H_{gg}(\alpha_s(Q)) \sum_{a,b} \left[ \phi_{a/A} \otimes C_{a \rightarrow g} \right] \otimes \left[ \phi_{b/B} \otimes C_{b \rightarrow g} \right] \times e^{-S(b, Q)}, \tag{27}$$

with  $H_{gg}(\alpha_s(Q)) = \sum_n H_{gg}^{(n)}(\alpha_s/\pi)^n$ , and the lowest order  $H_{gg}^{(0)} = 1$ . In analogy with parton distributions, the universal coefficient functions  $C_{i \rightarrow j}$  and the Sudakov form factor  $S(b, Q)$  can be defined by choosing a “resummation scheme”. The higher order contributions to the hard part,  $H_{gg}^{(n)}$ , can be calculated perturbatively. Since the reorganization affects only the perturbative part of  $W(b, Q, x_A, x_B)$ , our approach to extrapolate  $W_H^{\text{pert}}(b, Q, x_A, x_B)$  into the nonperturbative large  $b$  region, discussed in Sec. III. B, could also be used to calculate the  $Q_T$  distribution in this modification of the CSS formalism.

### III. ROLE OF THE REGION OF LARGE IMPACT PARAMETER

#### A. Suppressed role of the region of large $b$ at large $\sqrt{S}$

Prior to presenting alternative expressions for the extrapolation of  $W(b, Q, x_A, x_B)$  into the region of large  $b$ , we emphasize one important property of the  $b$ -space resummation formalism: the resummed exponential factor  $\exp[-S(b, Q)]$  suppresses the  $b$ -integrand in Eq. (3) when  $b$  is larger than  $1/Q$ . Therefore, when  $Q \gg \mu_0$ , the Fourier transform is dominated by a region of  $b$  much smaller than  $1/\mu_0$ , and the calculated  $Q_T$  distribution is insensitive to the non-perturbative information at large  $b$ .

Saddle-point methods are used in Refs. [24, 44] to show that for large enough  $Q$ , the Fourier transform in Eq. (3) is dominated by an impact parameter

$$b_{\text{SP}} \simeq \frac{1}{\Lambda_{\text{QCD}}} \left( \frac{\Lambda_{\text{QCD}}}{Q} \right)^\lambda, \quad (28)$$

where  $\lambda = 2A^{(1)}/(2A^{(1)} + \beta_0) \approx 0.61$  and  $\approx 0.41$ , for gluonic and fermionic processes, respectively, for  $n_f = 5$  quark flavors. This equation shows that the momentum scale corresponding to the saddle point,  $1/b_{\text{SP}}$ , should be within the perturbative region if  $Q$  is large enough. In Ref. [32], a more complete expression is derived for  $b_{\text{SP}}$  that takes into account the full  $b$  dependence of  $W_{ij}(b, c/b, x_A, x_B)$ .

The saddle point at  $Q_T = 0$  is determined from the differential equation

$$\frac{d}{db} \ln \left( b e^{-S(b, Q)} \right)_{b=b_0} + \frac{d}{db} \ln \left( \sum_{ij} \sigma_{ij \rightarrow hX}(Q) W_{ij}(b, \frac{c}{b}, x_A, x_B) \right)_{b=b_0} = 0. \quad (29)$$

If  $W_{ij}(b, c/b, x_A, x_B)$  has a weak dependence on  $b$  near  $b_0$ , the second term in Eq. (29) can be neglected, and the first term yields  $b_0 \approx b_{\text{SP}}$ . However, as we now show, the  $b$ -dependence of  $W_{ij}(b, c/b, x_A, x_B)$  is directly proportional to the evolution of the modified parton distributions.

The second term on the left-hand side of Eq. (29) can be expressed as

$$\frac{d}{db} \ln \left( \sigma_{gg}(Q) W_{gg}(b, \frac{c}{b}, x_A, x_B) \right) = \frac{d}{db} \left( \ln f_{g/A}(x_A, \mu, \frac{c}{b}) + \ln f_{g/B}(x_B, \mu, \frac{c}{b}) \right), \quad (30)$$

and

$$\frac{d}{db} f_{g/A}(x_A, \mu, \frac{c}{b}) = \frac{1}{b} \sum_a \int_{x_A}^1 \frac{d\xi}{\xi} \phi_{a/A}(\xi, \mu) \left[ \frac{d}{d \ln b} C_{a \rightarrow g}(\frac{x_A}{\xi}, \mu, \frac{c}{b}) \right]$$

$$\begin{aligned}
&\approx \frac{1}{b} \sum_a \int_{x_A}^1 \frac{d\xi}{\xi} \phi_{a/A}(\xi, \mu) \left[ -\frac{\alpha_s}{\pi} P_{a \rightarrow g}\left(\frac{x_A}{\xi}\right) \right] \\
&\approx -\frac{2}{b} \frac{d}{d \ln \mu^2} \phi_{g/A}(x_A, \mu) .
\end{aligned} \tag{31}$$

The derivative  $(d/d \ln \mu) \phi(x, \mu)$  is typically positive (negative) for  $x < x_0 \sim 0.1$  ( $x > x_0$ ), and the evolution is very steep when  $x$  is far from  $x_0$ . Correspondingly, the second term in Eq. (29) should be important when the relevant values of  $x_A \sim Q/\sqrt{S}$  and  $x_B \sim Q/\sqrt{S}$  are much smaller (or much greater) than  $x_0$ . At the LHC,  $x_A \sim x_B \sim 0.009$  for  $m_h = 125$  GeV.

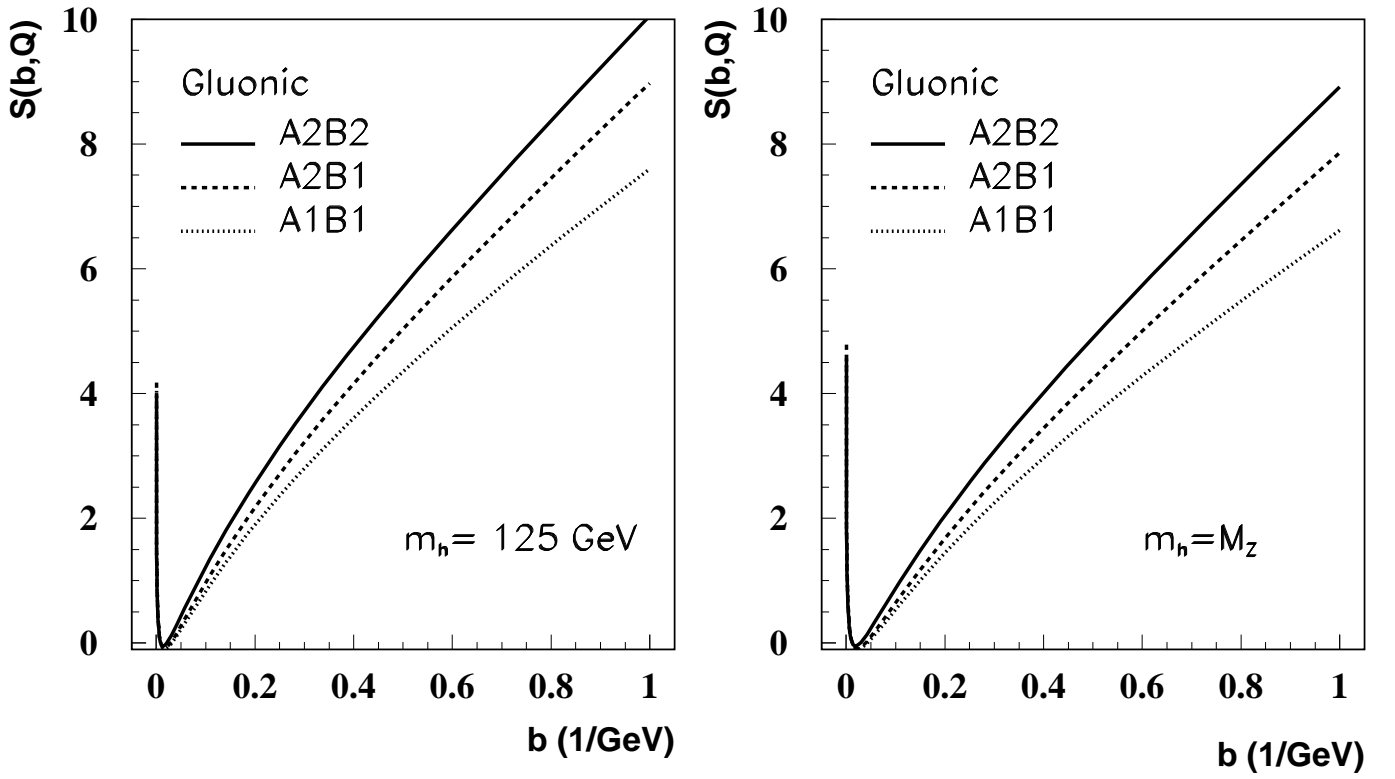


FIG. 1: The function  $S(b, Q)$  for Higgs boson production in gluon-gluon fusion at (a)  $Q = m_h = 125$  GeV and (b)  $m_h = M_Z$  as a function of impact parameter  $b$ . We show results for different orders of accuracy in the perturbative expansions of the functions  $A_g$  and  $B_g$ . The dotted curve is obtained with only the first order contributions  $A_g^{(1)}$  and  $B_g^{(1)}$  retained. For the dashed curve, we include  $A_g^{(2)}$  in addition, and for the solid curve, we keep all terms through  $A_g^{(2)}$  and  $B_g^{(2)}$  in Eq. (16).

The first term alone in Eq. (29) is a decreasing function of  $b$ . The derivative vanishes at  $b = b_{\text{SP}}$  producing a first approximation for the saddle point solution, Eq. (28). The negative sign in Eq. (31), and the fact that the number of small  $x$  partons increases when the scale

$\mu$  increases, mean that the second term in Eq. (29) is negative when  $x_A$  and  $x_B$  are smaller than the typical  $x_0$ . The full solution to Eq. (29) provides a saddle point that is less than the first approximation  $b = b_{\text{SP}}$ . (Conversely, at fixed-target energies where the typical  $x_A$  and  $x_B$  are greater than  $x_0$ , the typical  $b$  is greater than  $b_{\text{SP}}$ .) The numerical value for the saddle point depends strongly on  $\sqrt{S}$ , improving the predictive power of  $b$ -space resummation at large energies. When  $Q_T > 0$ , the Bessel function  $J_0(z = Q_T b)$  further suppresses the large  $b$  region of the  $b$ -integration. The suppression is greater for greater  $Q_T$ , and the  $b$ -space resummation formalism is expected to work progressively better for larger  $Q_T$ .

In the remainder of this subsection, we present figures that illustrate the  $b$  dependences of the Sudakov function  $S(b, Q)$  and of the factor  $bW(b, Q)$  in the integrand of Eq. (3), and we comment on their physical implications. The Sudakov function depends only on  $Q$  and on the perturbatively calculable functions  $A_g$  and  $B_g$ , Eqs. (15 - 19). Selecting  $Q = m_h = 125$  GeV, we show the behavior of  $S(b, m_h)$  in Fig. 1. The function has a pronounced minimum at very small  $b$ ,  $b \sim 0.02 \text{ GeV}^{-1}$ . Since it is  $\exp[-S(b, Q)]$  that enters the integrand, Fig. 1 shows that the Sudakov factor strongly suppresses both the large and small regions of  $b$ . It is instructive to examine the relative importance of next-to-leading order contributions in the functions  $A_g$  and  $B_g$ . As shown in the figure, it may be sufficient at very small  $b$  to retain only the first-order contributions,  $A_g^{(1)}$  and  $B_g^{(1)}$ . However, the second-order contributions, both  $A_g^{(2)}$  and  $B_g^{(2)}$ , are of growing relevance as  $b$  grows. The larger Sudakov function at large  $b$  in next-to-leading order means that the region of small  $Q_T$  is more suppressed, resulting in a shift of the peak of the distribution  $d\sigma/dy dQ_T$  to somewhat larger  $Q_T$  at higher orders. The large change associated with  $A_g^{(2)}$  may be understood because  $A_g$  in Eq. (19) is multiplied by  $\ln(Q^2)$ . It is possible that inclusion of  $A_g^{(3)}$ , once it is known, will produce important effects. A comparison of the results in Figs. 1(a) and (b) shows that the Sudakov function is peaked more narrowly at greater  $m_h$ . The suppression of the region of large  $b$  is more pronounced for larger  $m_h$ , again influencing a shift of the peak of the distribution  $d\sigma/dy dQ_T$  to somewhat larger  $Q_T$  as  $m_h$  is increased.

To examine the differences between  $Z$  production and Higgs boson production, we show in Fig. 2 the results appropriate for  $Z$  boson production, with  $Q = M_Z = 91.187$  GeV. The second-order fermionic function  $B_q^{(2)}$  plays a much less significant role in  $Z$  production than does the gluonic function  $B_g^{(2)}$  in Higgs boson production. Comparison of Figs. 1(b) and 2 shows that the gluonic Sudakov function is much larger than its quark counterpart, but



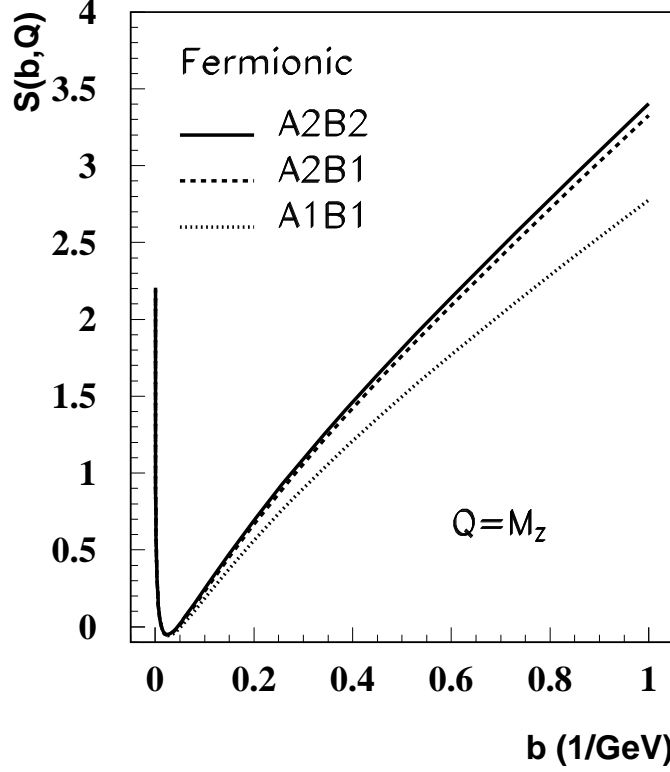


FIG. 2: The function  $S(b, Q)$  for  $Z$  boson production in as a function of impact parameter  $b$ . We show results for different orders of accuracy in the perturbative expansions of the functions  $A_g$  and  $B_g$ .

the curves are similar in shape otherwise. At  $b = 1$ , the ratio is about 2.5. The fact that the gluonic  $A_g$  and  $B_g$  functions are larger than their fermionic counterparts  $A_q$  and  $B_q$  is related to the differences in the values of the structure constants  $C_A$  and  $C_F$ . The larger color factor for gluons means that gluons radiate more readily. There will be more gluonic showering and correspondingly more suppression of the region of large  $b$  (*i.e.*, small  $Q_T$ ) when gluonic subprocesses are dominant. Greater suppression of the region of large  $b$  means that perturbation theory will have greater predictive power and resummed calculations will be more reliable for gluonic processes.

The all-orders resummed  $b$ -space function  $W(b, Q)$ , Eq. (26), depends on the choice of parton densities. We use the CTEQ5M set [45]. In Fig. 3, we show  $bW(b, Q)$  as a function of  $b$  at the energy of the LHC for two choices of the Higgs boson mass. This function is peaked sharply near  $b \sim 0.05 \text{ GeV}^{-1}$  (*c.f.*,  $Q_T \sim 20 \text{ GeV}$ ) well within the region of applicability of perturbative QCD. The function has essentially no support for  $b > 0.5 \text{ GeV}^{-1}$ . We expect,

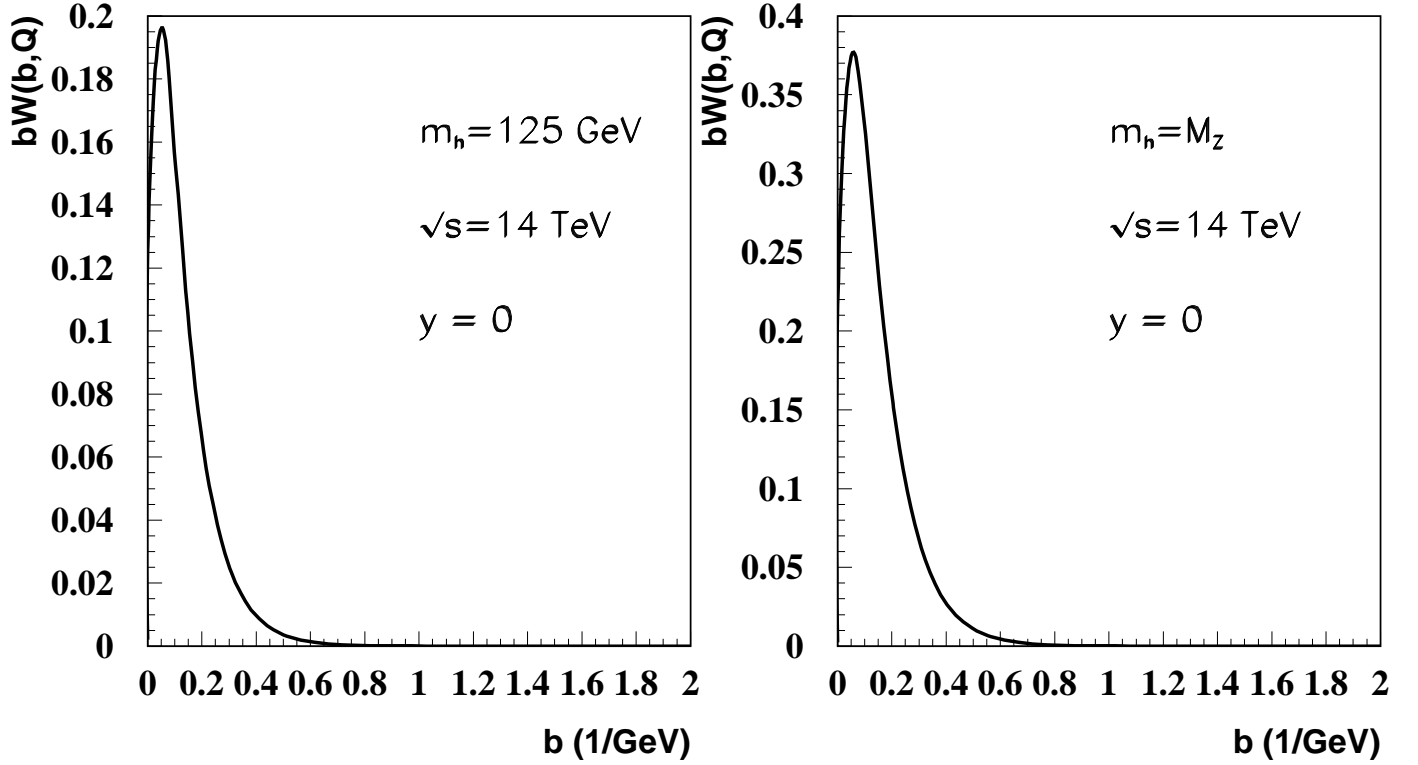


FIG. 3: The all-orders  $b$ -space resummed function  $bW(b, Q)$  for Higgs boson production in gluon-gluon fusion at  $\sqrt{S} = 14$  TeV for (a)  $Q = m_h = 125$  GeV and (b)  $m_h = M_Z$  as a function of impact parameter  $b$ .

therefore, that the non-perturbative input at large  $b$  will play a negligible role in Higgs boson production at LHC energies. Comparison of Figs. 3(a) and (b) demonstrates that the function is peaked somewhat more narrowly at larger  $m_h$ .

We present Fig. 4 to illustrate the difference in the resummed  $b$  space distributions for Higgs boson and  $Z$  boson production. In Figs. 3(b) and 4, we select the same mass  $Q = M_Z$  and collider energy  $\sqrt{S}$ . The function peaks near  $b \sim 0.12$  GeV $^{-1}$  for  $Z$  production, at about twice the value for Higgs boson production. The peak in the  $Q_T$  distribution will therefore occur at a smaller value of  $Q_T$  for  $Z$  production than for Higgs boson production. The significantly narrower distribution in  $b$  in the Higgs boson case is a reflection of the larger gluonic Sudakov factor. Predictions for the  $Q_T$  distribution of Higgs boson production are therefore expected to be less sensitive to non-perturbative physics than those for  $Z$  production, even if  $m_h = M_Z$ . (We note that at LHC energies, the typical values of  $x$  in the parton densities are  $\sim M_Z/\sqrt{S}$  and  $\sim m_h/\sqrt{S}$ . Even for  $m_h = 200$  GeV,  $x < 2 \times 10^{-2}$ . Therefore, production at the LHC is influenced by the behavior of parton densities at small  $x$ ,

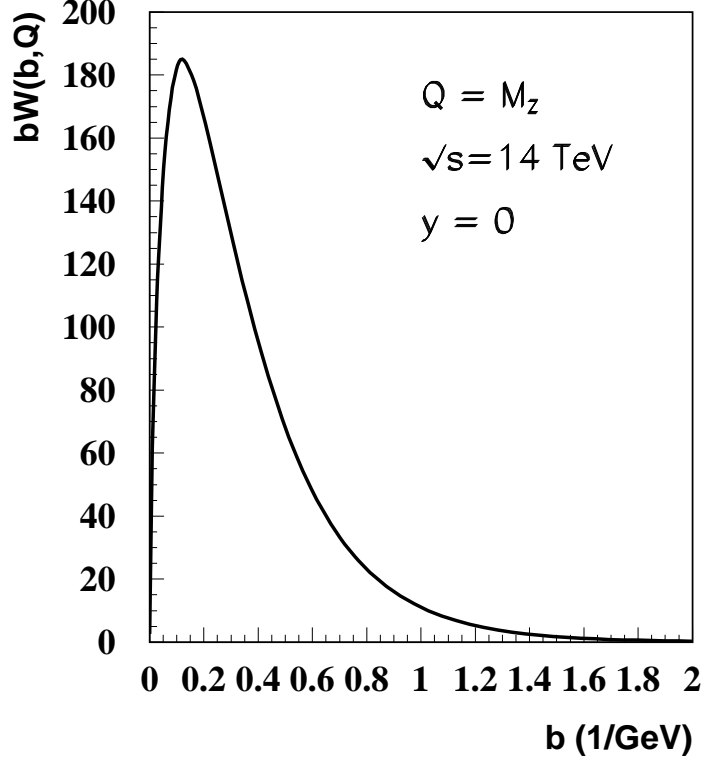


FIG. 4: The all-orders  $b$ -space resummed function  $bW(b, Q)$  for  $Z$  boson production at  $\sqrt{S} = 14$  TeV as a function of impact parameter  $b$ .

not at large  $x$  where the more rapid fall-off of the gluon density might otherwise make the  $Q_T$  distribution for Higgs boson production decrease more rapidly than that for  $Z$  production.)

### B. Extrapolation into the region of large- $b$

The perturbatively resummed function  $W(b, Q, x_A, x_B)$  in Eq. (3) is reliable only when  $b$  is small. An extrapolation into the region of large  $b$  is necessary in order to complete the Fourier transform in Eq. (3). In this section, we summarize different forms used in the literature for this extrapolation. The functional form of Qiu and Zhang [32] has the desirable property that it separates cleanly the perturbative prediction at small  $b$  from non-perturbative physics in the large  $b$  region.

In Ref. [24], a variable  $b_*$  is introduced along with a non-perturbative function  $F^{NP}(b, Q, x_A, x_B)$ ,

$$W^{\text{CSS}}(b, Q, x_A, x_B) \equiv W^{\text{pert}}(b_*, Q, x_A, x_B) F^{NP}(b, Q, x_A, x_B), \quad (32)$$

where  $b_* = b/\sqrt{1 + (b/b_{\max})^2} < b_{\max} = 0.5 \text{ GeV}^{-1}$ ;  $F^{NP}$  has a Gaussian-like dependence on  $b$ . The assumed non-perturbative distribution  $F^{NP}$  has the functional form [24]

$$F_{ij}^{NP}(b, Q, x_A, x_B) = \exp \left[ -\ln(Q^2 b_{\max}^2) g_1(b) - g_{i/A}(x_A, b) - g_{j/B}(x_B, b) \right]. \quad (33)$$

The  $\ln(Q^2)$  dependence is a prediction of the renormalization group equations. The functions  $g_1(b)$ ,  $g_{i/A}(x_A, b)$ , and  $g_{j/B}(x_B, b)$  are non-perturbative and assumed to vanish as  $b \rightarrow 0$ . The predictive power of the CSS formalism relies on the derived  $Q^2$  dependence and the universality of the functions  $F_{ij}^{NP}$ , fitted at one energy and used elsewhere.

Davies and Stirling (DS) proposed a simpler form for  $F^{NP}$  [26]

$$F_{DS}^{NP}(b, Q, x_A, x_B) = \exp \left[ -b^2 (g_1 + g_2 \ln(Qb_{\max}/2)) \right], \quad (34)$$

where  $g_1$  and  $g_2$  are flavor-independent fitting parameters. To incorporate possible  $\ln(\tau)$  dependence,  $\tau = Q^2/S = x_A x_B$ , Ladinsky and Yuan (LY) introduced an additional parameter  $g_3$  in a modified functional form [28]

$$F_{LY}^{NP}(b, Q, x_A, x_B) = \exp \left[ -b^2 (g_1 + g_2 \ln(Qb_{\max}/2)) - b g_1 g_3 \ln(100x_A x_B) \right]. \quad (35)$$

Similar to the DS parameterization, no flavor dependence is present. Landry, Brock, Ladinsky, and Yuan (LBLY) reported a global fit to the low energy Drell-Yan data as well as high energy  $W$  and  $Z$  data using both DS and LY parameterizations [33].

To preserve the predictive power of perturbative calculations, it is important that  $W^{\text{CSS}}(b, Q, x_A, x_B)$  be consistent with the perturbatively calculated  $W^{\text{pert}}(b, Q, x_A, x_B)$  when  $b < b_{\max}$ . However, use of the  $b_*$  variable necessarily alters the perturbatively calculated  $b$ -space distribution even within the perturbative region [32]. This alteration can be significant depending on the choice of the parametrization of  $F^{NP}$ . In the last subsection (c.f., Figs. 3 and 4), we argue that the  $Q_T$  distributions of  $W$ ,  $Z$ , and Higgs boson production at collider energies should not be sensitive to the large  $b$  tail of the spectrum. Any significant dependence on the fitting parameters would cast doubt on the predictive power of the  $b$ -space resummation formalism.

In Ref. [32], Qiu and Zhang introduce a new extrapolation

$$W(b, Q, x_A, x_B) = \begin{cases} W^{\text{pert}}(b, Q, x_A, x_B) & b \leq b_{\max} \\ W^{\text{pert}}(b_{\max}, Q, x_A, x_B) F^{NP}(b, Q; b_{\max}) & b > b_{\max}. \end{cases} \quad (36)$$

This expression manifestly preserves the QCD resummed  $b$ -space distribution in the perturbative region at small  $b$ . The authors also motivate the adoption of a new non-perturbative function in the region of large  $b$ :

$$F^{NP} = \exp \left\{ -\ln\left(\frac{Q^2 b_{\max}^2}{c^2}\right) \left[ g_1 \left( (b^2)^\alpha - (b_{\max}^2)^\alpha \right) + g_2 \left( b^2 - b_{\max}^2 \right) \right] - \bar{g}_2 \left( b^2 - b_{\max}^2 \right) \right\}. \quad (37)$$

The term proportional to  $(b^2)^\alpha$ , with  $\alpha < 1/2$ , corresponds to a direct extrapolation of the resummed  $W^{\text{pert}}(b, Q, x_A, x_B)$ . The parameters,  $g_1$  and  $\alpha$  are fixed in relation to  $W^{\text{pert}}$  by the requirement that the first and second derivatives of  $W(b, Q, x_A, x_B)$  be continuous at  $b = b_{\max}$ . Dependence on  $x_A$  and  $x_B$  is included in the parameters  $g_1$  and  $\alpha$ . The terms proportional to  $b^2$  correspond to inverse-power corrections to the evolution equation. Power corrections from soft gluon showers are the origin of the  $g_2$  term, and non-vanishing intrinsic transverse momenta of the incident partons lead to the  $\bar{g}_2$  term. The values of  $g_2$  and  $\bar{g}_2$  are unknown and must be obtained from fits to data.

In Fig. 5 we present ratios of the functions  $bW(b, Q)$  in use by different groups. In Fig. 5(a), the numerator is the two-parameter form of Davies and Stirling, whereas in Fig. 5(b) it is the three-parameter functional form adopted by Ladinsky and Yuan, Eqs. (32) and (35). However, in both cases we use the updated parameters of Landry *et al* and the CTEQ5M parton densities. The denominator in the ratios is the Qiu and Zhang function we use in this paper, Eqs. (36) and (37), with  $b_{\max} = 0.5$ ,  $g_2 = 0$ , and  $\bar{g}_2 = 0$ . For  $Z$  production at the energy of the Tevatron, the ratios do not deviate from 1 by more than 20% as long as  $b < 0.5$ , as might be expected because all groups provide acceptable fits to data. However, very significant deviations from 1 are evident at the energy of the LHC, notably in the region  $b < 0.5$  where purely perturbative physics should be dominant. The deviations reach 100% for  $b \sim 0.4$ . This comparison shows explicitly the influence within the purely perturbative region of the use of the variable  $b_*$  and the nonperturbative function  $F^{NP}$  in Eq. (32).

Figure 5 shows that the deviations from the perturbatively calculated  $W^{\text{pert}}(b, Q)$  depend strongly on the collision energy  $\sqrt{S}$ . This energy dependence is an artifact of the use of the variable  $b_*$ . Since  $b_* < b$  for all  $b \neq 0$ , the shifted  $b$ -space distribution  $W^{\text{pert}}(b_*, Q) < W^{\text{pert}}(b, Q)$  for values of  $b$  smaller than the location of saddle point, and  $W^{\text{pert}}(b_*, Q) > W^{\text{pert}}(b, Q)$  for  $b$  larger than the saddle point. The magnitude of the difference between the  $W^{\text{pert}}(b_*, Q)$  and  $W^{\text{pert}}(b, Q)$  depends on the shape of  $W^{\text{pert}}(b, Q)$ . When  $\sqrt{S}$  increases,

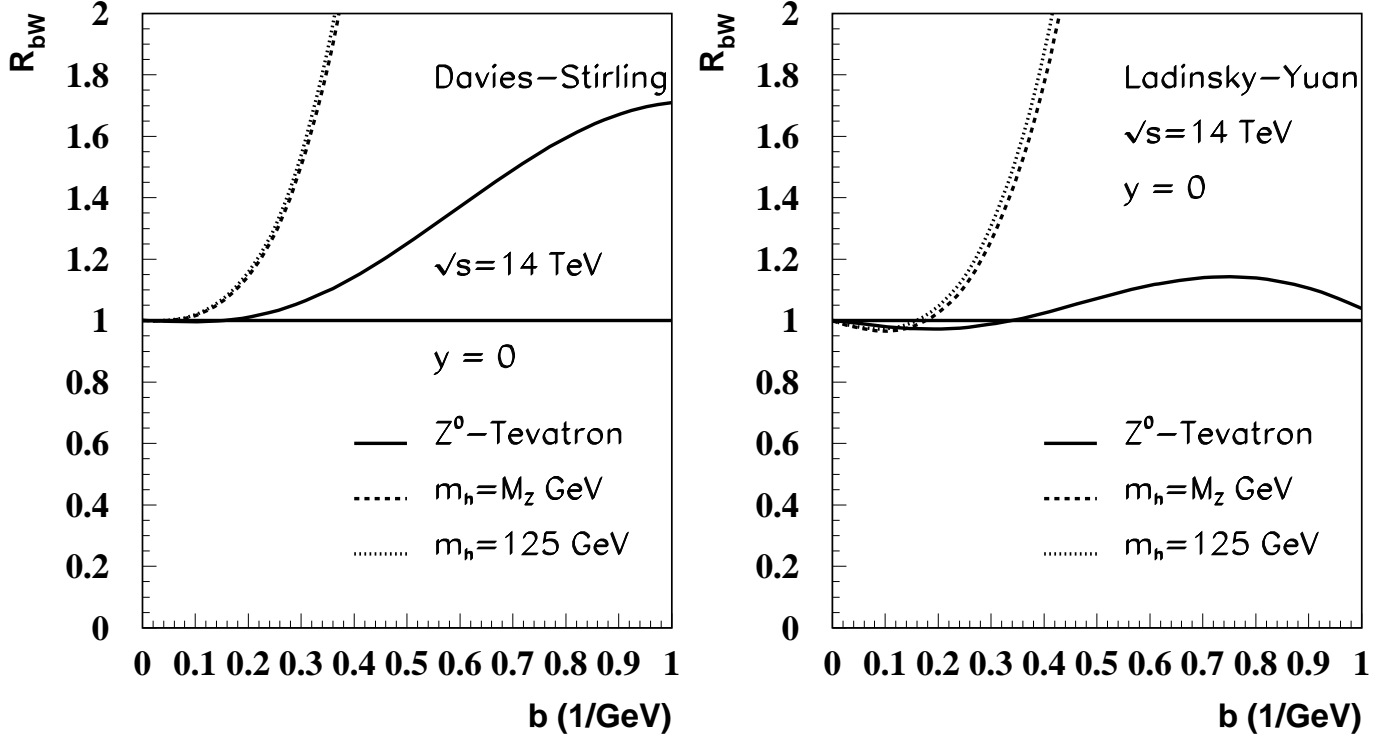


FIG. 5: Ratios of the functions  $bW(b, Q)$ . Comparisons are shown of (a) the DS parametrization and (b) the LY choice with respect to the function we use in this paper. The solid lines show the comparisons for  $Z$  production at the energy of the Fermilab Tevatron,  $\sqrt{S} = 1.8$  TeV. The dashed and dotted lines show the ratios for Higgs boson production at the LHC.

$W^{\text{pert}}(b, Q)$  becomes narrower, and its much steeper behavior leads to a larger deviation of  $W^{\text{pert}}(b_*, Q)$  from  $W^{\text{pert}}(b, Q)$ . The use of either the DS or the LY parameterizations in  $W^{\text{CSS}}(b, Q)$ , Eq. (32), leads to a reduction in the region  $b < 0.2$  and strong enhancement in the region  $b > 0.2$ . Once the Fourier transform is made to  $Q_T$  space, the net effects of these two differences are a shift to smaller  $Q_T$  in the location of the predicted maximum of the distribution  $d\sigma/dy dQ_T$  and a narrowing of the predicted peak in this distribution.

#### IV. EXPRESSIONS FOR THE FIXED-ORDER CONTRIBUTIONS IN PERTURBATIVE QCD

Working at fixed-order in QCD perturbation theory [19, 20, 21, 22], one can express the differential cross section for Higgs boson production in the form of a convolution

$$\begin{aligned} \frac{d\sigma_{AB \rightarrow hX}^{(\text{pert})}}{dQ^2 dy dQ_T^2} &= \sigma_{gg \rightarrow hX}^{(0)} \sum_{ab} \int_{x_A}^1 \frac{d\xi_A}{\xi_A} \int_{x_B}^1 \frac{d\xi_B}{\xi_B} \phi_{a/A}(\xi_A, \mu) \phi_{b/B}(\xi_B, \mu) \\ &\quad \times H_{ab \rightarrow hX}(Q_T, Q, \frac{x_A}{\xi_A}, \frac{x_B}{\xi_B}, \alpha_s(\mu), \mu). \end{aligned} \quad (38)$$

In this expression,  $\sigma_{gg \rightarrow hX}^{(0)}$  is the cross section given in Eq. (8). The functions  $\phi_{a/A}(x_A, \mu)$  and  $\phi_{b/B}(x_B, \mu)$  are probabilities that incident partons  $a$  and  $b$  from hadrons  $A$  and  $B$  carry fractional light-cone momenta  $x_A$  and  $x_B$ , respectively, at factorization scale  $\mu$ . The parton level hard-scattering function  $H_{ab \rightarrow hX}(Q_T, Q, x_A/\xi_A, x_B/\xi_B, \alpha_s(\mu), \mu)$  is expanded in a power-series in the strong coupling strength  $\alpha_s$

$$H_{ab \rightarrow hX} = \sum_{n=0} H_{ab \rightarrow hX}^{(n)} \left( \frac{\alpha_s(\mu)}{\pi} \right)^n. \quad (39)$$

The lowest order contribution ( $n = 0$ ),  $gg \rightarrow h$  comes from the top-quark loop, and, in the absence of partonic intrinsic transverse momentum, it yields a distribution that is a  $\delta$ -function in transverse momentum  $Q_T$

$$H_{gg}^{(0)} = \delta \left( 1 - \frac{x_A}{\xi_A} \right) \delta \left( 1 - \frac{x_B}{\xi_B} \right) \delta^2(Q_T). \quad (40)$$

At first-order in  $\alpha_s$ , there are virtual loop-corrections to the subprocess  $gg \rightarrow h$  along with contributions in which two partons interact to produce a parton plus the Higgs boson. Labelling these 2-to-2 contributions by the tree-subprocesses, we write the functions  $H_{ab \rightarrow hX}^{(1)}$  in terms of partonic Mandelstam variables  $\hat{s}$ ,  $\hat{t}$ , and  $\hat{u}$  as [19]

*gluon-gluon*  $gg \rightarrow hq$ :

$$H_{gg}^{(1)} = \frac{1}{2\pi} C_A \left[ \frac{\hat{s}^4 + \hat{t}^4 + \hat{u}^4 + Q^8}{\hat{s} \hat{t} \hat{u} Q^2} \right] \delta(\hat{s} + \hat{t} + \hat{u} - Q^2), \quad (41)$$

*gluon-quark(antiquark)*  $gq \rightarrow hq$  ( $g\bar{q} \rightarrow h\bar{q}$ ):

$$H_{gq}^{(1)} = \frac{1}{2\pi} C_F \left[ \frac{\hat{s}^2 + \hat{u}^2}{-\hat{t} Q^2} \right] \delta(\hat{s} + \hat{t} + \hat{u} - Q^2), \quad (42)$$

*quark(antiquark)-gluon*  $qg \rightarrow hq$  ( $\bar{q}g \rightarrow h\bar{q}$ ):

$$H_{qg}^{(1)} = \frac{1}{2\pi} C_F \left[ \frac{\hat{s}^2 + \hat{t}^2}{-\hat{u} Q^2} \right] \delta(\hat{s} + \hat{t} + \hat{u} - Q^2), \quad (43)$$

and the s-channel *quark-antiquark* subprocess  $q\bar{q} \rightarrow hg$ :

$$H_{q\bar{q}}^{(1)} = \frac{1}{2\pi} \left( \frac{C_F}{C_A} (N^2 - 1) \right) \left[ \frac{\hat{t}^2 + \hat{u}^2}{\hat{s} Q^2} \right] \delta(\hat{s} + \hat{t} + \hat{u} - Q^2). \quad (44)$$

The first-order contributions from  $gg$ ,  $qg$ , and  $gq$  scattering are all singular as  $Q_T \rightarrow 0$ . Following convention, we use the word “asymptotic” to designate the terms that are at least as singular as  $Q_T^{-2}$ . This asymptotic contribution may be written in analogy to Eq. (38) as the convolution

$$\begin{aligned} \frac{d\sigma_{AB \rightarrow hX}^{(\text{asym})}}{dQ^2 dy dQ_T^2} &= \sigma_{gg \rightarrow hX}^{(0)} \sum_{ab} \int_{x_A}^1 \frac{d\xi_A}{\xi_A} \int_{x_B}^1 \frac{d\xi_B}{\xi_B} \phi_{a/A}(\xi_A, \mu) \phi_{b/B}(\xi_B, \mu) \\ &\quad \times w_{ab \rightarrow hX}(Q_T, Q, \frac{x_A}{\xi_A}, \frac{x_B}{\xi_B}, \alpha_s(\mu), \mu). \end{aligned} \quad (45)$$

Expanded in a power series in  $\alpha_s$ , the asymptotic partonic hard part  $w_{ab \rightarrow hX}$  becomes

$$w_{ab \rightarrow hX} = \sum_{n=1} w_{ab \rightarrow hX}^{(n)} \left( \frac{\alpha_s(\mu)}{\pi} \right)^n. \quad (46)$$

The lowest order asymptotic contributions ( $n = 0$ ) vanish for  $Q_T > 0$ ,

$$w_{ab}^{(0)} = 0. \quad (47)$$

Categorizing the first-order contributions as before, we write the asymptotic forms as *gluon-gluon*:

$$\begin{aligned} w_{gg}^{(1)} &= \frac{1}{2\pi} \frac{1}{Q_T^2} \left\{ 2\delta(1 - z_A)\delta(1 - z_B) \left[ A_g^{(1)} \log\left(\frac{Q^2}{Q_T^2}\right) + B_g^{(1)} \right] \right. \\ &\quad \left. + \delta(1 - z_A) P_{g \rightarrow g}(z_B) + \delta(1 - z_B) P_{g \rightarrow g}(z_A) \right\}, \end{aligned} \quad (48)$$

where

$$z_A = \frac{x_A}{\xi_A}, \quad \text{and} \quad z_B = \frac{x_B}{\xi_B}. \quad (49)$$

The forms are simpler for the other subprocesses.

*gluon-quark(antiquark)*:

$$w_{gq}^{(1)} = \frac{1}{2\pi} \frac{1}{Q_T^2} \{ \delta(1 - z_A) P_{q \rightarrow g}(z_B) \}, \quad (50)$$



*quark(antiquark)-gluon:*

$$w_{qg}^{(1)} = \frac{1}{2\pi} \frac{1}{Q_T^2} \{ \delta(1 - z_B) P_{q \rightarrow g}(z_A) \}, \quad (51)$$

and *quark-antiquark:*

$$w_{q\bar{q}}^{(1)} = 0. \quad (52)$$

As discussed in Sec. II, resummation treats only the parts of the fixed-order QCD expressions that are at least as singular as  $Q_T^{-2}$  in the limit  $Q_T \rightarrow 0$ . The remainder is

$$\begin{aligned} \frac{d\sigma_{AB \rightarrow hX}^{(Y)}}{dQ^2 dy dQ_T^2} &= \sigma_{gg \rightarrow hX}^{(0)} \sum_{ab} \int_{x_A}^1 \frac{d\xi_A}{\xi_A} \int_{x_B}^1 \frac{d\xi_B}{\xi_B} \phi_{a/A}(\xi_A, \mu) \phi_{b/B}(\xi_B, \mu) \\ &\times R_{ab \rightarrow hX}(Q_T, Q, \frac{x_A}{\xi_A}, \frac{x_B}{\xi_B}, \alpha_s(\mu), \mu). \end{aligned} \quad (53)$$

As a power-series expansion in  $\alpha_s$ , the partonic hard part for the remainder term is

$$R_{ab \rightarrow hX} = \sum_{n=0} R_{ab \rightarrow hX}^{(n)} \left( \frac{\alpha_s(\mu)}{\pi} \right)^n, \quad (54)$$

where

$$R_{ab \rightarrow hX}^{(n)} = H_{ab \rightarrow hX}^{(n)} - w_{ab \rightarrow hX}^{(n)}. \quad (55)$$

In our numerical work presented in Sec. V, we use order  $\alpha_s$  expressions for  $H_{ab \rightarrow hX}^{(n)}$ . In subsequent investigations, one might incorporate the NLO results [21, 22].

## V. PREDICTIONS

In this section we present our predictions for the transverse momentum distribution of Higgs boson production in proton-proton collisions at the LHC energy  $\sqrt{S} = 14$  TeV. We provide results at both fixed rapidity  $y = 0$  and for the cross section integrated over the rapidity range  $|y| \leq 2.4$ . To illustrate interesting differences, we also show our results for  $Z$  boson production at the same energy [34]. Our predictions are based on Eqs. (2), (3), (26), and (53). We employ expressions for the parton-level hard-scattering functions valid through first-order in  $\alpha_s$ , Eqs. (40) - (44), with the asymptotic forms Eqs. (47) - (52). For  $A_g$  and  $B_g$  in the Sudakov factor, Eq. (19), we take the expansion valid through second order ( $n = 2$ ), Eq. (16). For the coefficient functions in the modified parton densities, we use the expansion

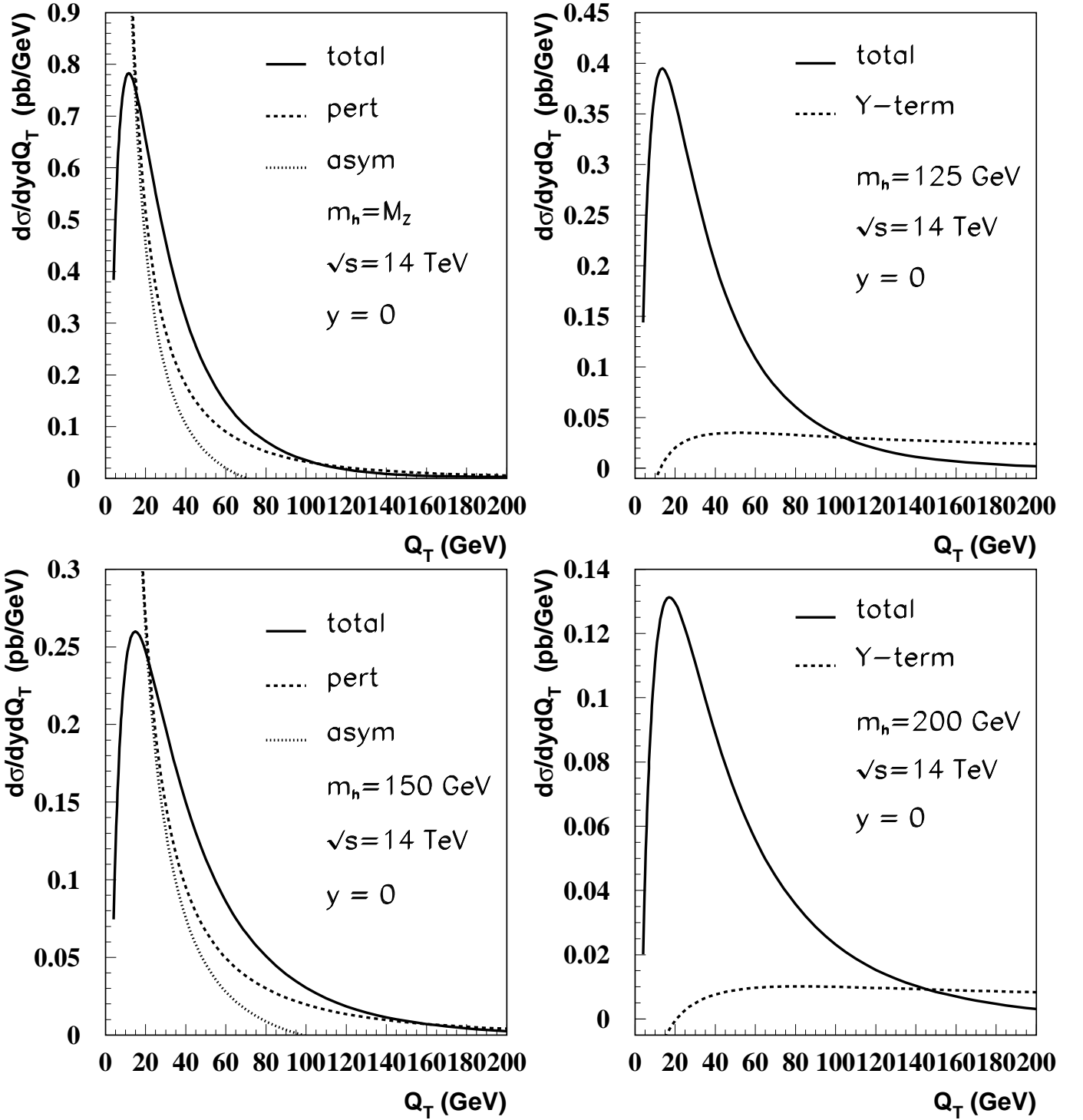


FIG. 6: Differential cross section  $d\sigma/dy dQ_T$  for Higgs boson production at  $\sqrt{s} = 14$  TeV and fixed rapidity  $y = 0$  with (a)  $Q = M_Z$ , (b)  $Q = m_h = 125$  GeV, (c)  $Q = m_h = 150$  GeV, and (d)  $Q = m_h = 200$  GeV, as a function of transverse momentum  $Q_T$ . The total prediction is shown as a solid line. In (a) and (c), the fixed-order perturbative calculation is shown as a dashed line and its asymptotic limit as a dotted line. In (b) and (d), the contribution from the remainder  $Y$  term is shown as a dashed line.

through  $n = 1$ , Eq. (23). (Our results are therefore consistently at next-to-leading-logarithm (NLL) accuracy). We use a next-to-leading order form for  $\alpha_s(\mu)$  and next-to-leading order normal parton densities  $\phi(x, \mu)$  [45]. In the fixed-order perturbative expressions that enter the “Y” function, we select a fixed renormalization/factorization scale  $\mu = \kappa\sqrt{m_h^2 + Q_T^2}$ , with  $\kappa = 0.5$ . For the resummed term, we take as our central value  $\mu = c/b$ , with  $c = 2e^{-\gamma_E}$ . To show sensitivity to the choice of  $\mu$ , we also compute cross sections with the choices  $\mu = 0.5\sqrt{m_h^2 + Q_T^2}$  and  $\mu = 2\sqrt{m_h^2 + Q_T^2}$ .

The extrapolation into the non-perturbative region of large  $b$  is accomplished with Eqs. (36) and (37). As remarked before, the parameters  $g_1$  and  $\alpha$  in Eq. (37) are fixed in relation to  $W^{\text{pert}}$  by the requirement that the first and second derivatives of  $W(b, Q, x_A, x_B)$  be continuous at  $b = b_{\text{max}} = 0.5 \text{ GeV}^{-1}$ . Since, as shown in Sec. III A, there is little sensitivity to the region of large  $b$ , we adopt for most of our results the values  $g_2 = 0$  and  $\bar{g}_2 = 0$  in Eq. (37). However, to demonstrate the insensitivity numerically, we also present results for other choices of  $b_{\text{max}}$ ,  $g_2$ , and  $\bar{g}_2$ .

In the limit  $Q_T \rightarrow 0$ , sub-dominant singularities produce a mismatch [24] between the complete fixed-order expressions in Eqs. (41) - (44) and their asymptotic forms in Eqs. (48) - (52). Sub-leading divergences drive the difference towards a negative infinity as  $Q_T \rightarrow 0$ . The “Y” term is not large in the region of small  $Q_T$ , but the singularity in the limit  $Q_T \rightarrow 0$  is sufficiently strong that it can pull the sum in Eq. (2) to negative values in the region of very small  $Q_T$ . There are various possible remedies for this difficulty, including introduction of an off-set in  $Q_T$  in the “Y” function. In our numerical work, we use a parameter  $Q_T^{\text{min}}$ , replacing  $Q_T$  in the “Y” function only by  $\sqrt{Q_T^2 + (Q_T^{\text{min}})^2}$ . In keeping with CSS, we select  $Q_T^{\text{min}} = 0.3 \text{ GeV}$  as our central value and show the sensitivity of results to choices ranging from  $Q_T^{\text{min}} = 0$  to  $Q_T^{\text{min}} = 0.5 \text{ GeV}$ .

The Bessel function in the integrand of Eq. (3) is an oscillatory function, and a high degree of numerical accuracy is necessary to ensure accurate cancellations. The number of oscillations depends strongly on the value of  $Q_T$ . When  $b \in (0, 2) \text{ GeV}^{-1}$ , the number of times  $J_0(Q_T b)$  crosses zero is 0, 6, 63, and 127 for  $Q_T = 1, 10, 100$ , and  $200 \text{ GeV}$ , respectively. Following Qiu and Zhang, we use an integral form for the Bessel function

$$J_0(z) = \frac{1}{\pi} \int_0^\pi \cos(z \sin(\theta)) d\theta. \quad (56)$$

Overall numerical accuracy is controlled by improving the accuracy of the integration in

Eq. (56).

### A. $Q_T$ distributions for Higgs boson and $Z$ production

We display our predicted  $Q_T$  distributions for Higgs boson production at the LHC in Figs. 6 and 7, respectively. In Fig. 6, we show  $d\sigma/dy dQ_T$  as a function of  $Q_T$  at fixed rapidity  $y = 0$ , whereas in Fig. 7, we show the  $Q_T$  distributions for rapidity integrated over the interval  $|y| < 2.4$ . (The choice  $|y| < 2.4$  is motivated by the expected acceptance of the LHC detectors for photons [7].) We present results for four choices of mass of the Higgs boson, values that span the range of present interest in the SM,  $m_h = M_Z = 91.187$  GeV,  $m_h = 125$  GeV,  $m_h = 150$  GeV (where the  $WW^*$  decay channel is dominant), and  $m_h = 200$  GeV (above both  $WW$  and  $ZZ$  decay thresholds). In all cases, the solid lines represent the total prediction, Eq. (2). In Figs. 6(a) and (c), as well as in Figs. 7(a) and (c), we also show the fixed-order purely perturbative result and its  $Q_T \rightarrow 0$  asymptotic form. In Figs. 6(b) and (d), as well as in Figs. 7(b) and (d), we show instead the contribution from the fixed-order remainder “ $Y$ ” term.

In Figs. 6(a) and (c), we observe the divergence as  $Q_T \rightarrow 0$  of the fixed-order purely perturbative result and the expected numerical equality of the purely perturbative result and its  $Q_T \rightarrow 0$  asymptotic form at small  $Q_T$ . The asymptotic form falls away more rapidly with  $Q_T$ . Figures 6(b) and (d) demonstrate that the total prediction, Eq. (2), is clearly dominated by the all-orders resummed term for  $Q_T \leq Q$ . At larger  $Q_T$ , the  $Y$  term is comparable in size. In the expression for  $Y$ , we use the order- $\alpha_s$  QCD expressions. Next-to-leading order contributions tend to alter theoretical predictions, and, correspondingly, we would expect that our predictions would change somewhat for  $Q_T > Q$  if higher order contributions are included. In Figs. 6(b) and (d), we also observe that the  $Y$  term becomes negative at small  $Q_T$ , as we discuss above.

The resummed result (labeled “total”) makes a smooth transition to the fixed-order perturbative result near or just above  $Q_T = Q$ , for all  $Q$ , without need of a supplementary matching procedure. With all  $Q_T$  distributions extended to  $Q_T = 200$  GeV, our implementation of the resummation formalism works smoothly throughout the  $Q_T$  region even for the distributions differential in rapidity,  $d\sigma/dy dQ_T$ . The transition from the resummed distribution to the fixed-order perturbative contribution is continuous and much less ambiguous

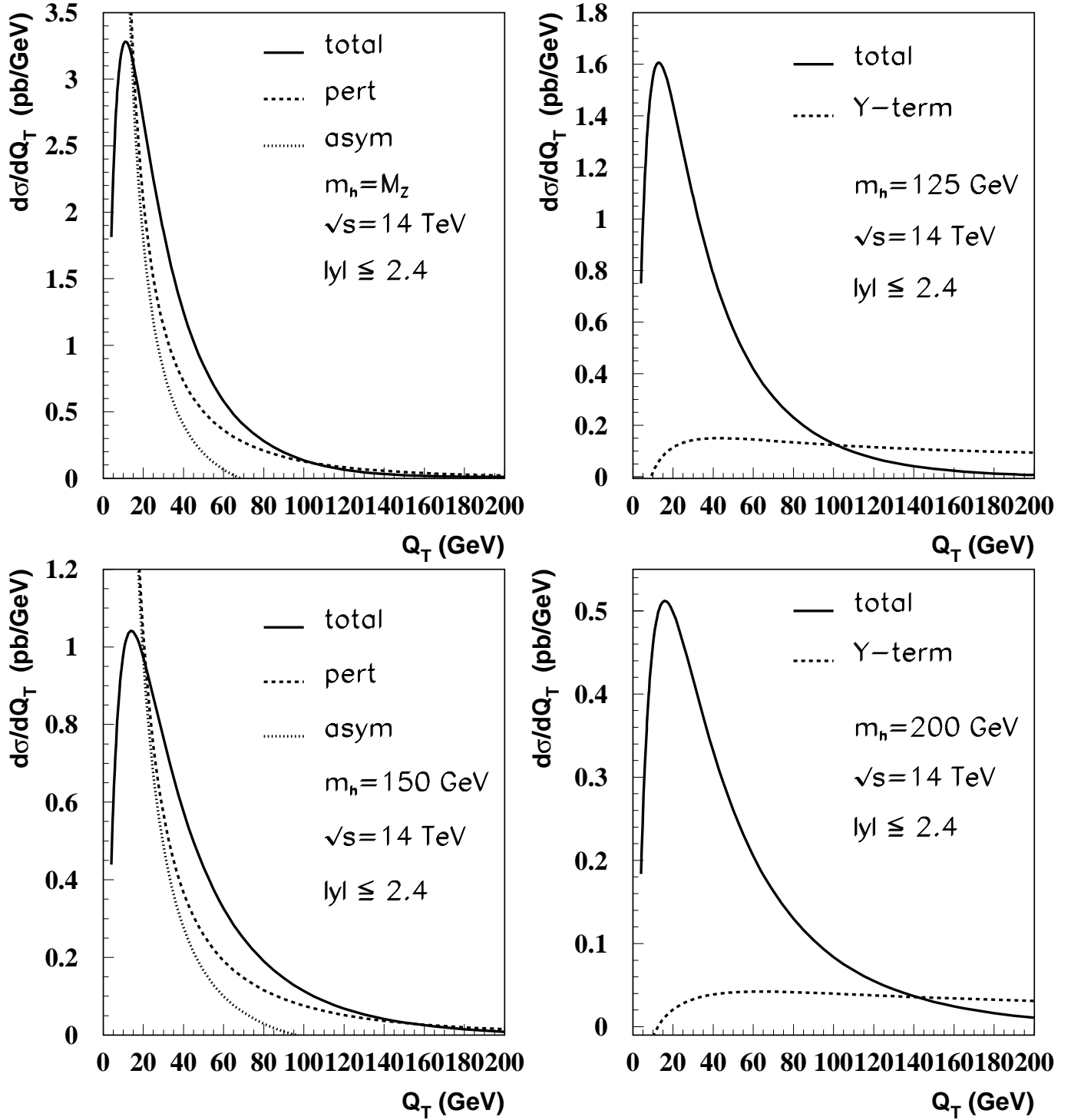


FIG. 7: Differential cross section  $d\sigma/dQ_T$  for Higgs boson production at  $\sqrt{s} = 14$  TeV with rapidity integrated over the interval  $|y| < 2.4$  with (a)  $Q = M_Z$ , (b)  $Q = m_h = 125$  GeV, (c)  $Q = m_h = 150$  GeV, and (d)  $Q = m_h = 200$  GeV, as a function of transverse momentum  $Q_T$ . The total prediction is shown as a solid line. In (a) and (c), the fixed-order perturbative calculation is shown as a dashed line and its asymptotic limit as a dotted line. In (b) and (d), the contribution from the remainder  $Y$  term is shown as a dashed line.

than is sometimes seen in the literature.

We note that the resummed results for Higgs boson production begin to fall below the fixed-order perturbative expectations when  $Q_T$  exceeds  $Q$ . This effect is likely associated with the logarithmic dependence  $\ln(Q/Q_T)$  in Eq. (48). A similar effect is not seen in our predictions for  $Z$  boson production where the fermionic coefficient  $A_q^{(1)}$  is smaller than the gluonic coefficient  $A_g^{(1)}$ . The fixed-order result should provide the correct theoretical answer for  $Q_T \sim Q$  (and above) where only one large momentum scale is present and large logarithmic effects proportional to  $\ln(Q/Q_T)$  are insignificant. We adopt the fixed-order result as our best estimate of the theoretical prediction wherever it is larger than the resummed result in the region  $Q_T > Q$ .

We display our predicted  $Q_T$  distributions for  $Z$  boson production at the LHC in Figs. 8. The resummed distributions are very smooth functions of  $Q_T$  over the full range shown and they converge without discontinuity with the fixed-order perturbative results above  $Q_T = M_Z$ . No supplementary matching is employed.

Two points are evident in the comparison of  $Z$  boson and Higgs boson production, with  $m_h = M_Z$ . The peak in the  $Q_T$  distribution occurs at a smaller value of  $Q_T$  for  $Z$  production. At  $y = 0$ , the curve peaks at  $Q_T \sim 4.8$  GeV for  $Z$  production and at  $Q_T \sim 11.6$  GeV for Higgs boson production. Second, the distribution is narrower for  $Z$  production, falling to half its maximum by  $Q_T \sim 16$  GeV, whereas the half-maximum for Higgs production is not reached until  $Q_T \sim 35$  GeV. Technically, both differences are a direct reflection of the differences in the functions  $bW(b, Q)$  discussed in Sec. III A. The  $b$ -space distribution is narrower for Higgs boson production and peaks at smaller  $b$ . Correspondingly, since  $Q_T \sim 1/b$ , the  $Q_T$  distribution is broader and peaks at larger  $Q_T$ . The physics behind this important difference is that the larger QCD color factors produce more gluonic showering in the glue-gluon scattering subprocess that dominates inclusive Higgs boson production than in the fermionic subprocesses relevant for  $Z$  production. After all-orders resummation, the enhanced showering suppresses the large- $b$  (small  $Q_T$ ) region more effectively for Higgs boson production.

Comparison of the predicted  $Q_T$  distributions for Higgs boson production at different masses of the Higgs boson shows that the peak of the distribution shifts to greater  $Q_T$  as  $m_h$  grows and that the distribution broadens somewhat. At  $y = 0$ , the peaks are centered at about  $Q_T = 11.6, 13.6, 14.9$ , and  $17.2$  GeV for  $m_h = M_Z, 125, 150$ , and  $200$  GeV,

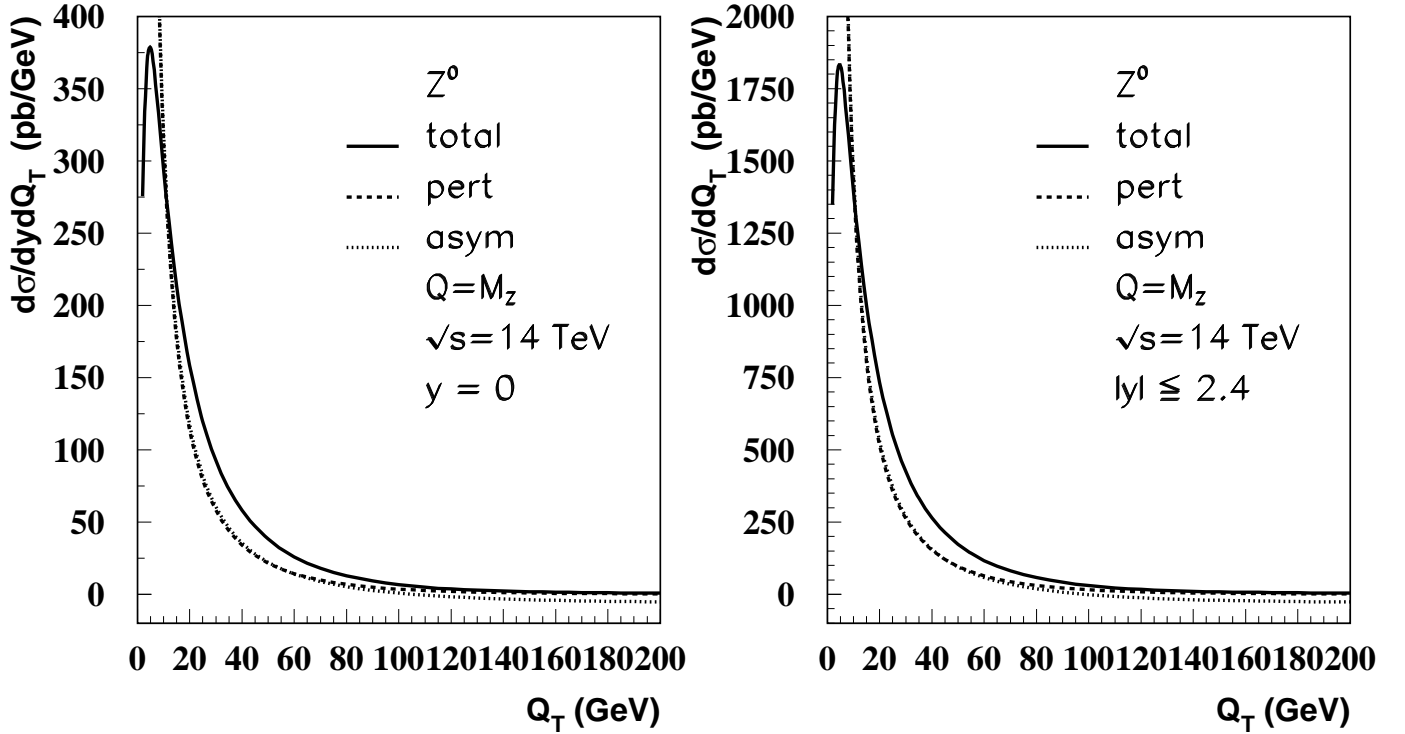


FIG. 8: Differential cross section  $d\sigma/dy dQ_T$  as a function of transverse momentum  $Q_T$  for  $Z$  boson production at  $\sqrt{S} = 14$  TeV and (a) fixed rapidity  $y = 0$  and (b)  $|y| < 2.4$ . Shown are the total prediction as a solid line, the fixed-order perturbative calculation as a dashed line, and the asymptotic limit as a dotted line.

respectively. The mass dependence for both Higgs and  $Z$  boson production is illustrated in Fig. 9. For  $Z^*$  boson masses above the physical value  $M_Z$  we assume that the production model is unchanged except for the difference in mass of the  $Z^*$ . The peak position at  $y = 0$  is at 5.5 GeV for  $M_{Z^*} = 200$  GeV.

The change of the  $Q_T$  distribution with  $m_h$  can also be represented quantitatively with plots of the mean value  $\langle Q_T \rangle$  and of the root-mean-square  $\langle Q_T^2 \rangle^{\frac{1}{2}}$ , shown in Fig. 10. Because of the long tail of the distribution  $d\sigma/dQ_T$  at large  $Q_T$ , the mean value  $\langle Q_T \rangle$  is about 3.6 times the value of  $Q_T$  at which the peak occurs in the distribution. We observe that  $\langle Q_T \rangle$  grows from about 41 GeV at  $m_h = M_Z$  to about 65 GeV at  $m_h = 200$  GeV. The curve is nearly a straight line over the range shown, with  $\langle Q_T \rangle \simeq 0.21m_h + 22$  GeV. In computing the averages, we switch from the “total” result for  $d\sigma/dy dQ_T$  shown, for example, in Fig. 6 to the fixed-order perturbative result when the fixed-order answer is the larger of the two choices above  $Q_T = Q$ . We extend our numerical integrations to  $Q_T = 2$  TeV in

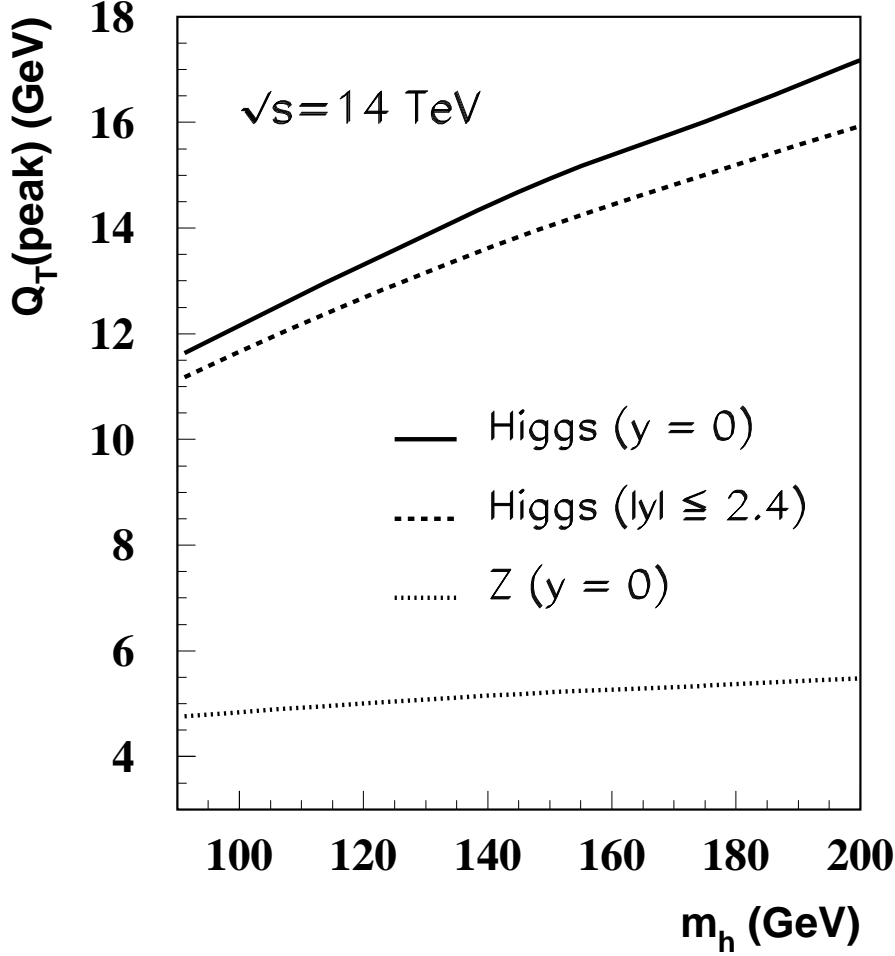


FIG. 9: Location of the peaks of the transverse momentum distributions for Higgs boson and  $Z^*$  boson production as a function of Higgs boson mass at  $\sqrt{S} = 14$  TeV. For Higgs boson production we show results at fixed rapidity  $y = 0$  and for  $y$  integrated over the interval  $|y| \leq 2.4$ .

the case of  $\langle Q_T \rangle$  and to  $Q_T = 5$  TeV for  $\langle Q_T^2 \rangle$  in order to achieve insensitivity of the results to the upper limit of integration. The nearly linear growth of  $\langle Q_T \rangle$  and of  $\langle Q_T^2 \rangle^{1/2}$  with  $m_h$  is a reflection of the fact that the peak location in  $Q_T$  of the distribution  $d\sigma/dy dQ_T$  grows in nearly linear fashion as  $m_h$  increases. Since  $Q_T \sim 1/b$ , the expression for the saddle point, Eq. (28), suggests that  $\langle Q_T \rangle \propto 1/b_{\text{SP}} \propto m_h^\lambda$ , with fractional power  $\lambda$ , rather than a nearly linear behavior. We remark that for large  $m_h$ , a linear fit is a good approximation to the fractional power dependence over a restricted range in  $m_h$ .

For comparison with our results for Higgs boson production, we quote our predictions for  $Z$  production:  $\langle Q_T \rangle = 25$  GeV and  $\langle Q_T^2 \rangle^{1/2} = 38$  GeV. We note that the difference  $\langle Q_T^h \rangle - \langle Q_T^Z \rangle \simeq 16$  GeV at  $m_h = M_Z$ , a manifestation of more significant gluonic



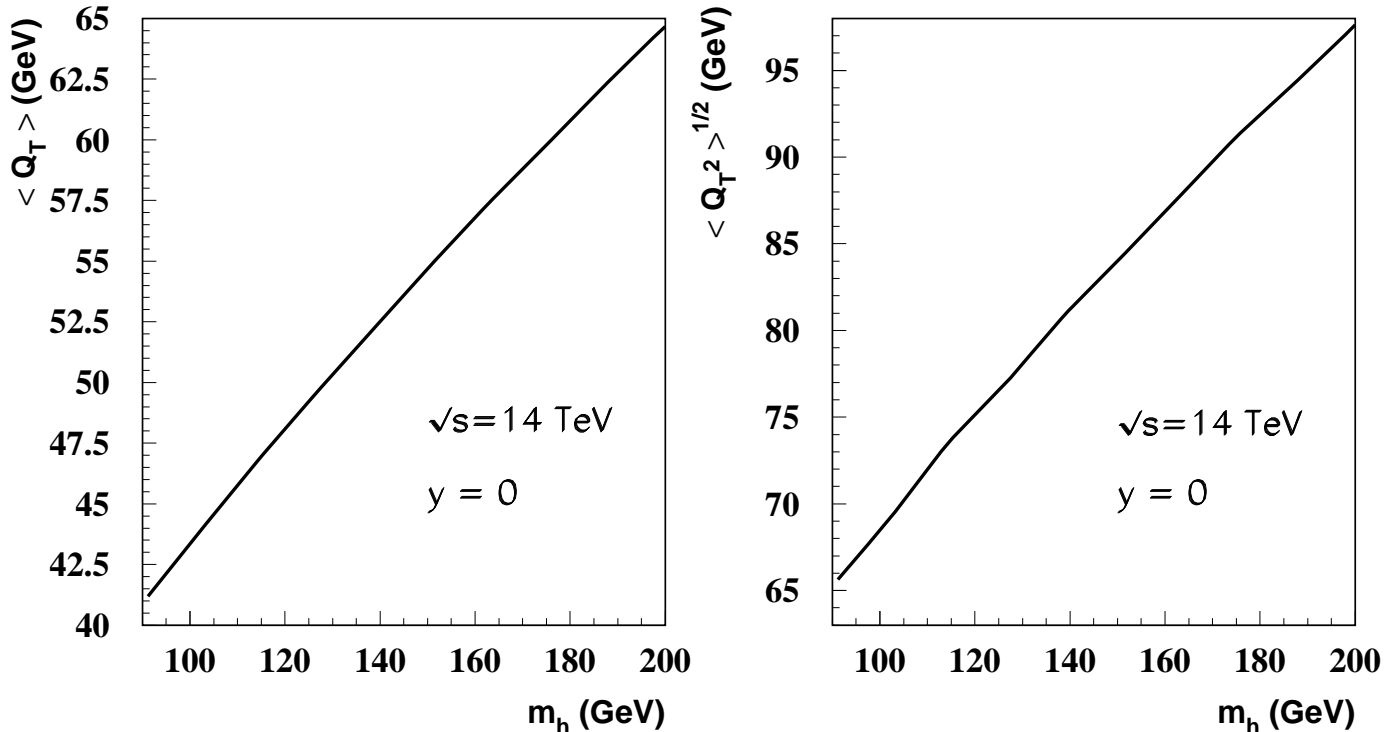


FIG. 10: Predictions of (a) the average value of the transverse momentum and (b) the root-mean-square for Higgs boson production as a function of Higgs boson mass at  $\sqrt{S} = 14 \text{ TeV}$  and fixed rapidity  $y = 0$ . We show results for Higgs boson masses  $m_h$  from  $M_Z$  to 200 GeV.

radiation in Higgs boson production. The harder  $Q_T$  spectrum suggests that the signal to background ratio can be enhanced if Higgs bosons are selected with large  $Q_T$ , a point to which we return in Sec. VI.

Choices of variable parameters are made in obtaining our results, and it is important to examine the sensitivity of the results to these choices. The parameter choices include the specification of the renormalization/factorization scale  $\mu$ , the non-perturbative input, and  $Q_T^{\min}$ . Uncertainties of a different sort are associated with the order in perturbation theory at which we work.

Dependence on the renormalization/factorization scale  $\mu$  is often a good indicator of theoretical uncertainty. In Fig. 11, we show this dependence for the differential cross section  $d\sigma/dQ_T$  at Higgs boson mass  $m_h = 125 \text{ GeV}$ . Since we are interested principally in examining scale dependence of the resummed result, we fix the scale in the purely perturbative remainder term Eq. (53) to be  $\mu = 0.5\sqrt{m_h^2 + Q_T^2}$ . This term is not important in the region of modest  $Q_T$  where the cross section is large. We present results for three choices

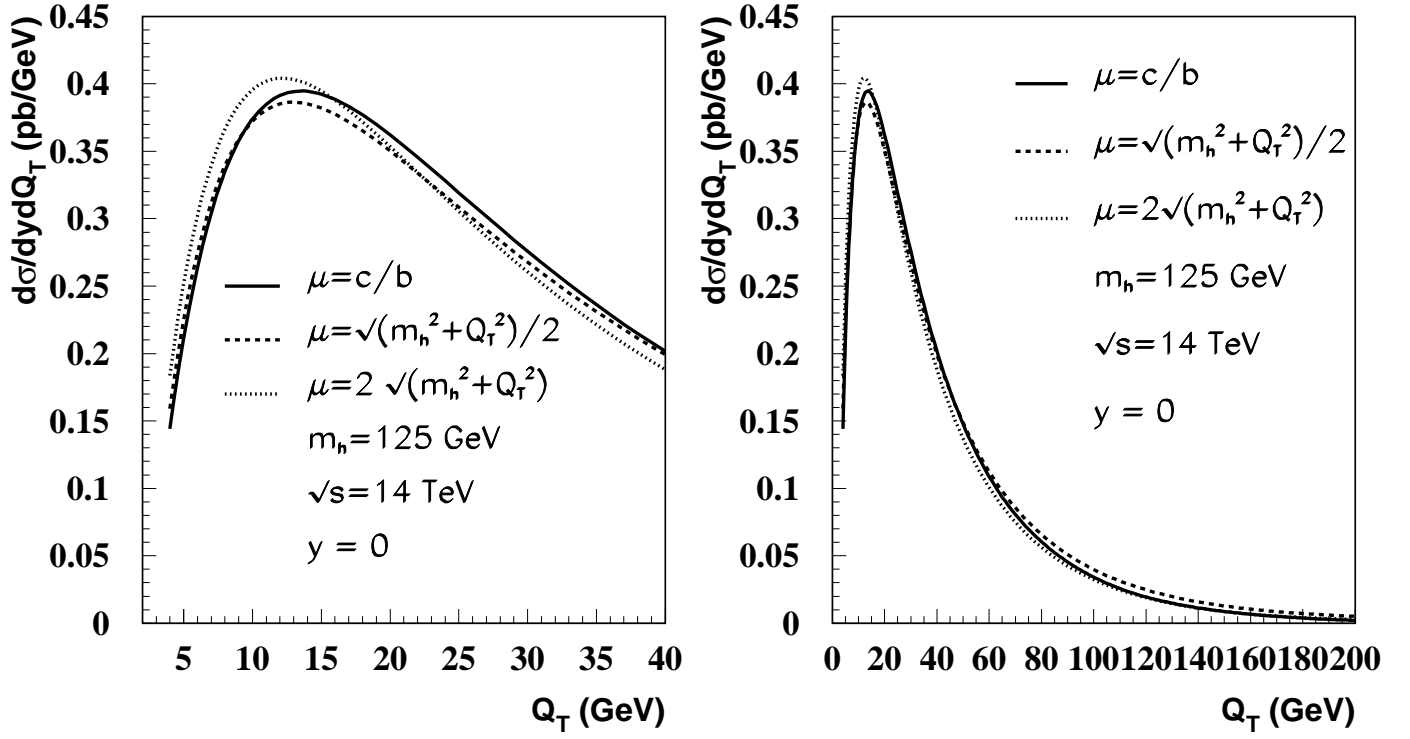


FIG. 11: Renormalization/factorization scale  $\mu$  dependence of the differential cross section  $d\sigma/dy dQ_T$  as a function of  $Q_T$  for Higgs boson mass  $m_h = 125$  GeV at  $\sqrt{S} = 14$  TeV and fixed rapidity  $y = 0$ . We show results for three choices of the scale. In (a) the region of low and intermediate  $Q_T$  is shown in expanded form to illustrate the variation of the position in  $Q_T$  of the maximum of the distribution.

of the scale in the resummed term, Eqs. (3) and (26). All these results are obtained with  $Q_T^{\min} = 0.3$  GeV. We select as default choice  $\mu = c/b$  with  $c = 2e^{-\gamma_E}$  such that the scale varies with the integration variable  $b$ . The other two choices are independent of  $b$  but are proportional to the hard-scale of the collision,  $\mu = 0.5\sqrt{m_h^2 + Q_T^2}$  and  $\mu = 2\sqrt{m_h^2 + Q_T^2}$ . Scale dependence is not insignificant in the region where the distribution is large. It can shift the position of the peak by about 1.5 GeV, with corresponding changes in the normalization of the distribution above and below the position of the peak. The value of  $d\sigma/dy dQ_T$  at the peak position is shifted by 4 to 5%. The shift in the location of the peak is about the same as the shift that occurs between resummation done at leading-logarithmic (LL) accuracy and at NLL accuracy [46].

The parameter  $Q_T^{\min}$  is necessary to prevent the “Y” function from pulling the total result negative at very small  $Q_T$ . For our central results we select  $Q_T^{\min} = 0.3$  GeV. We examine

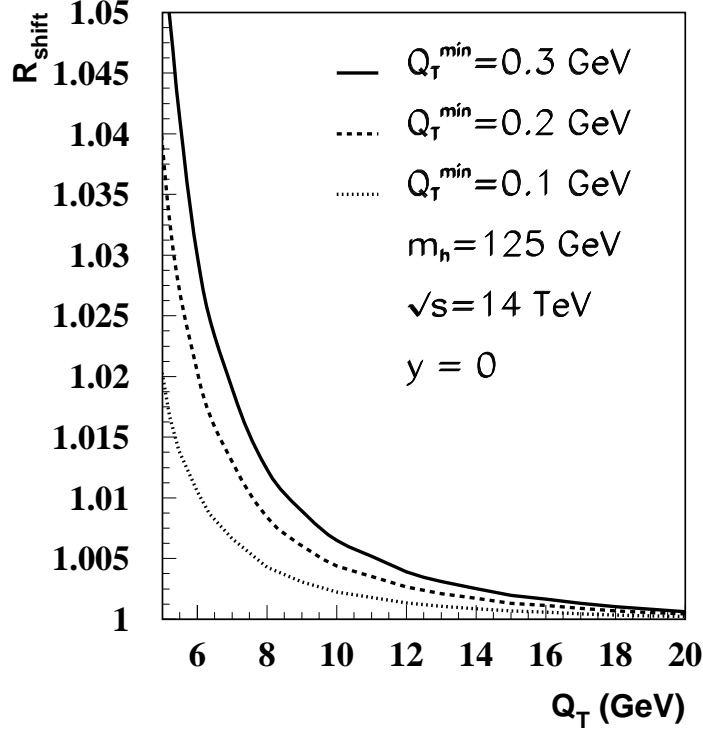


FIG. 12: *Dependence of the differential cross section  $d\sigma/dy dQ_T$  on the parameter  $Q_T^{\min}$  as a function of  $Q_T$  for Higgs boson mass  $m_h = 125$  GeV at  $\sqrt{s} = 14$  TeV and fixed rapidity  $y = 0$ . We show results for three values of  $Q_T^{\min}$ , divided by the results for  $Q_T^{\min} = 0$ .*

changes associated with this parameter in Fig. 12. The ratio shown is

$$R_{\text{shift}} = \frac{d\sigma}{dy dQ_T}(Q_T^{\min}) / \frac{d\sigma}{dy dQ_T}(Q_T^{\min} = 0). \quad (57)$$

We vary  $Q_T^{\min}$  over the range 0 to 300 MeV. The position of the peak of the  $Q_T$  distribution is very stable; within a bin width of 1 GeV, there is no change in the location of the peak. At  $m_h = 125$  GeV the change in the value of  $d\sigma/dy dQ_T$  at the peak location of  $\sim 13.6$  GeV is only 0.3% when  $Q_T^{\min}$  varies from 0 to 0.3 GeV. However, for  $Q_T < 4$  GeV, the uncertainties are much larger. One message from this exercise is that the resummed  $Q_T$  distribution cannot be computed reliably when  $Q_T \ll Q_T^{\text{peak}}$ , a conclusion that should not be surprising. On the other hand, the uncertainties in the  $Q_T$  distribution in the region of small  $Q_T$  associated with the choice of  $Q_T^{\min}$  should not be worse than potential uncertainties in the data.

In Fig. 13 we examine the dependence of our predictions on the choice of the non-perturbative parameters  $b_{\text{max}}$ ,  $g_2$ , and  $\bar{g}_2$ . We combine the dependence on the latter two parameters in a function  $G2 = g_2 \ln(Q^2 b_{\text{max}}^2 / c^2) + \bar{g}_2$ , defined in Ref. [32]. In Fig. 13(a) we

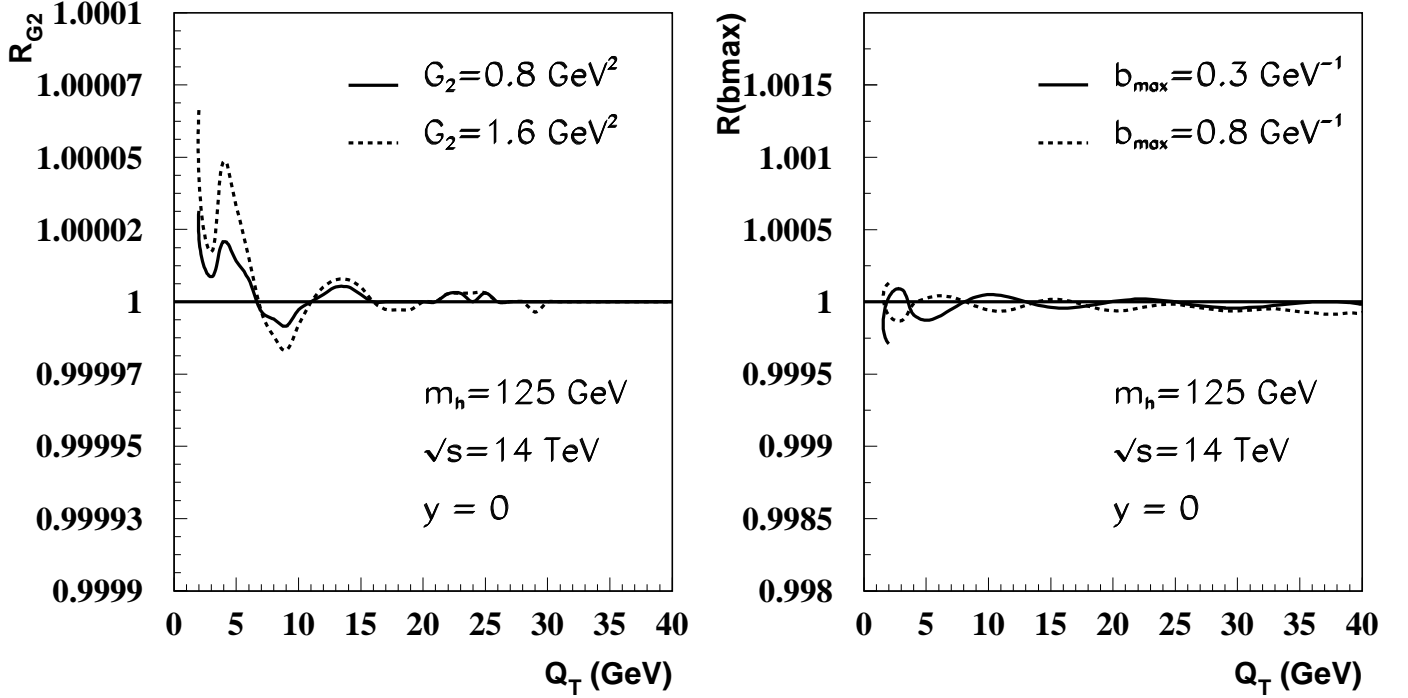


FIG. 13: Dependence of the differential cross section  $d\sigma/dy dQ_T$  on the non-perturbative parameters (a)  $G_2$  and (b)  $b_{\text{max}}$  as a function of  $Q_T$  for Higgs boson mass  $m_h = 125 \text{ GeV}$  at  $\sqrt{S} = 14 \text{ TeV}$  and fixed rapidity  $y = 0$ . We show results for two choices of each parameter.

plot the ratio of the  $Q_T$  distribution with residual power corrections over its value without these contributions. In Ref. [32],  $G_2 = 0.4 \text{ GeV}^2$  is shown to produce the best fit to Tevatron data on  $W$  and  $Z$  boson production. To enhance the possible influence of power corrections, we choose parameters that are a few times larger than are needed in  $W$  and  $Z$  production. In Fig. 13(a), the values  $G_2 = 0.8 \text{ GeV}^2$  and  $1.6 \text{ GeV}^2$  are used, twice- and four-times the values determined earlier. The corresponding changes in the predictions for Higgs boson production are very small. In Fig. 13(b), we examine sensitivities to the choice of  $b_{\text{max}}$ . The ratio displayed is  $R(b_{\text{max}}) = d\sigma/dy dQ_T(b_{\text{max}})/d\sigma/dy dQ_T(b_{\text{max}} = 0.5 \text{ GeV}^{-1})$ . For changes in  $b_{\text{max}}$  between 0.3 and  $0.8 \text{ GeV}^{-1}$ , the uncertainties in our predictions are much less than 1%. They are consistent with the level of accuracy of our numerical computations. Evident in Fig. 13 is that the formulation we use to describe the non-perturbative region has no effect on the behavior of differential cross section at large  $Q_T$ .

Comparison of Figs. 11 and 13 shows that uncertainties related to scale variation are greater than uncertainties associated with non-perturbative physics. Uncertainties associated with physics in the region of large  $b$  are at most 1 to 2% depending on the size of the

power corrections we introduce, whereas scale dependence can change distributions by more than 10%, if one examines the spectrum as a whole, and by about 5% in the region of the peak. Non-perturbative effects vanish very quickly as  $Q_T$  increases, while sensitivity to the scale choice increases as  $Q_T$  increases. Variations associated with non-perturbative physics in the large  $b$  region are much smaller at LHC energies than higher-order corrections to the perturbative functions  $A$ ,  $B$ , and  $C$ .

Before closing this section, we comment on differences between our results and previously published predictions of resummed  $Q_T$  spectra for Higgs boson production at LHC energies. In particular, the locations of the maxima in the distributions  $d\sigma/dy dQ_T$  obtained from the *ResBos* Monte Carlo generator [30] (*c.f.*, Figs. 6 and 7 of Ref. [46]) occur at somewhat smaller values of  $Q_T$  and the distributions themselves differ as a function of  $Q_T$  above the location of the maximum. These differences are anticipated in our discussion towards the end of Sec. III. The differences arise from the different approach for extrapolating  $W^{\text{pert}}(b, Q)$  into the non-perturbative region at large  $b$ . In our case, the extrapolation has the desirable property that it does not affect the physics in the perturbative region  $b < b_{\text{max}} \sim 0.5$  GeV.

A different resummation scheme, such as discussed in Ref. [43], can lead to uncertainties similar to those shown in Fig. 11 of this paper and in Fig. 7 of Ref. [46]. Because our method for extrapolation into the nonperturbative large  $b$  region is different, we expect the locations of the maxima in the distributions  $d\sigma/dy dQ_T$  in Fig. 7 of Ref. [46] to shift to somewhat larger values of  $Q_T$ .

## VI. CONCLUSIONS

Discovery of the Higgs particle is essential to shed light on the mechanism of electroweak symmetry breaking. The partonic subprocess  $g+g \rightarrow hX$  dominates Higgs boson production in hadronic reactions when the Higgs boson mass is in the expected range  $m_h < 200$  GeV. The two-scale nature of the production dynamics, with mass  $m_h$  and transverse momentum  $Q_T$  both potentially large, and the fact that the fixed-order perturbative QCD contributions are singular as  $Q_T \rightarrow 0$ , necessitates all-orders resummation of large logarithmic contributions in order to obtain meaningful predictions for the  $Q_T$  distribution particularly in the region of modest  $Q_T$  where the cross section is largest. We perform this resummation of multiple soft-gluon emissions using an impact parameter  $b$ -space formalism. At LHC energies,

the typical values of the incident parton momentum fractions  $x_A \sim x_B \sim m_h/\sqrt{S} \sim 0.009$  (for  $m_h = 125$  GeV) are small, and the gluon distribution evolves steeply at small  $x$ . Consequently, the saddle point in  $b$  of the Fourier transform from  $b$ -space to  $Q_T$  space is well into the region of perturbative validity. The resummed  $Q_T$  distributions are therefore determined primarily by the perturbatively calculated  $b$ -space distributions at small  $b$ , with negligible contributions from the non-perturbative region of large  $b$ . Our resummation formalism has excellent predictive power for the  $Q_T$  distributions of Higgs boson and  $Z$  production at the LHC energy,  $\sqrt{S} = 14$  TeV, for  $Q_T$  as large as the respective boson masses  $Q$ . Matching between the resummed and fixed-order calculations at large  $Q_T$  is unambiguous in the method we employ. An examination of the numerical sensitivity of our results to variations in the renormalization/factorization scale  $\mu$  and to parameters associated with the form of the assumed non-perturbative function at large  $b$  shows the expected modest dependence of  $\mu$  and essentially no dependence on the non-perturbative parameters, except in the region of extremely small  $Q_T$ .

In this paper, we present predictions for the  $Q_T$  distributions of Higgs boson and  $Z$  production at  $\sqrt{S} = 14$  TeV. Results are shown in Figs. 6 - 10. At the same mass,  $m_h = M_Z$ , the predicted mean value  $\langle Q_T \rangle$  is about 16 GeV larger for Higgs boson production than for  $Z$  boson production. For the Higgs boson,  $\langle Q_T \rangle$  grows from about 41 GeV at  $m_h = M_Z$  to about 65 GeV at  $m_h = 200$  GeV, and the root-mean-square  $\langle Q_T^2 \rangle^{1/2}$  from about 65 GeV to about 98 GeV.

Searches for the Higgs boson in its decay to two photons require an excellent understanding of the production characteristics of both the signal and backgrounds. The primary background to direct photon production comes from decays of hadrons such as  $\pi^0$ ,  $\eta^0$ , and  $\omega^0$ , themselves produced copiously at large transverse momentum from the fragmentation of jets, as well as from misidentified photons (*e.g.*, from processes that produce two jets or a jet and a photon and in which jets are misidentified as photons). Even after excellent photon/jet discrimination and application of photon isolation restrictions, simulations show ratios of the expected signal to irreducible backgrounds in the range of 4 to  $5 \times 10^{-2}$  for  $m_h$  in the interval 120 to 130 GeV [7]. The irreducible backgrounds arise from the QCD annihilation  $q\bar{q} \rightarrow \gamma\gamma$ , the Compton  $qg \rightarrow \gamma\gamma q$  (with one of the final photons produced from parton fragmentation (generalized bremsstrahlung)), and the gluon box  $gg \rightarrow \gamma\gamma$  subprocesses, and their counterparts at higher orders of perturbation theory [13, 14, 15]. Although

there is some dependence on the di-photon invariant mass and photon transverse momentum, the contributions of the annihilation and gluon box processes are comparable, and the fragmentation processes make a smaller contribution than either of these others. Of interest to us is the expected dependence of the ratio of signal to irreducible background. In this paper we provide predictions for the transverse momentum distribution of the signal. The gluon box subprocess has the same initial state as the inclusive gluon fusion process that produces the Higgs boson. Consequently, for di-photon invariant mass  $M_{\gamma\gamma} = m_h$ , we expect that the transverse momentum spectrum of the gluon box contribution to the irreducible background will have the same shape after soft gluon resummation as that for the Higgs boson. However, the other major component of the irreducible background, the annihilation  $q\bar{q} \rightarrow \gamma\gamma$  subprocess, has the same initial state structure as  $Z$  boson production. As we show in this paper, the  $Q_T$  spectrum of  $Z$  production is predicted to be softer than that for Higgs boson production (*c.f.*, Figs. 9 and 10). We suggest therefore that a selection of events with large  $Q_T^{\gamma\gamma}$  could help in significantly improving the signal to background ratio.

## ACKNOWLEDGMENTS

Research in the High Energy Physics Division at Argonne is supported by the United States Department of Energy, Division of High Energy Physics, under Contract W-31-109-ENG-38. JWQ is supported in part by the United States Department of Energy under Grant No. DE-FG02-87ER40371. JWQ acknowledges the hospitality of the Argonne high energy physics theory group while part of this research was being carried out. ELB acknowledges the hospitality of the Aspen Center for Physics where part of this work was done.

- 
- [1] J. F. Gunion and H. E. Haber, Nucl. Phys. B **272**, 1 (1986) [Erratum-ibid. B **402**, 567 (1986)].
  - [2] ALEPH Collaboration, R. Barate *et al.*, Phys. Lett. B **495**, 1 (2000) [arXiv:hep-ex/0011045];  
DELPHI Collaboration, P. Abreu *et al.*, Phys. Lett. B **499**, 23 (2001) [arXiv:hep-ex/0102036];  
OPAL Collaboration, G. Abbiendi *et al.*, Phys. Lett. B **499**, 38 (2001) [arXiv:hep-ex/0101014];  
L3 Collaboration, M. Acciarri *et al.*, Phys. Lett. B **508**, 225 (2001) [arXiv:hep-ex/0012019];  
LEP Higgs Working Group for Higgs boson searches Collaboration, “Search for the standard model Higgs boson at LEP,” arXiv:hep-ex/0107029, published in *Budapest 2001, High Energy*

- Physics*, Proceedings of the International Europhysics Conference on High Energy Physics (HEP 2001), Budapest, Hungary, July 12-18, 2001, and “Searches for the neutral Higgs bosons of the MSSM: Preliminary combined results using LEP data collected at energies up to 209-GeV,” arXiv:hep-ex/0107030.
- [3] LEP Higgs Working Group for Higgs boson searches Collaboration, “Flavor independent search for hadronically decaying neutral Higgs bosons at LEP,” arXiv:hep-ex/0107034.
  - [4] The LEP Collaborations: ALEPH Collaboration, DELPHI Collaboration, L3 Collaboration, OPAL Collaboration, the LEP Electroweak Working Group, the SLD Heavy Flavour, Electroweak Working Group, D. Abbaneo *et al.*, “A combination of preliminary electroweak measurements and constraints on the standard model,” arXiv:hep-ex/0112021.
  - [5] S. Heinemeyer, W. Hollik, and G. Weiglein, Phys. Rev. D **58**, 091701 (1998) [arXiv:hep-ph/9803277]; Phys. Lett. B **440**, 296 (1998) [arXiv:hep-ph/9807423]; Eur. Phys. J. C **9**, 343 (1999) [arXiv:hep-ph/9812472]; M. Carena, M. Quiros, and C. E. M. Wagner, Nucl. Phys. B **461**, 407 (1996) [arXiv:hep-ph/9508343]; H. E. Haber, R. Hempfling, and A. H. Hoang, Z. Phys. C **75**, 539 (1997) [arXiv:hep-ph/9609331]; J. R. Espinosa and R. J. Zhang, J. High Energy Phys. **0003**, 026 (2000) [arXiv:hep-ph/9912236]; Nucl. Phys. B **586**, 3 (2000) [arXiv:hep-ph/0003246]; M. Carena, H. E. Haber, S. Heinemeyer, W. Hollik, C. E. M. Wagner, and G. Weiglein, Nucl. Phys. B **580**, 29 (2000) [arXiv:hep-ph/0001002]; G. Degrandi, P. Slavich, and F. Zwirner, Nucl. Phys. B **611**, 403 (2001) [arXiv:hep-ph/0105096]; A. Brignole, G. Degrandi, P. Slavich, and F. Zwirner, Nucl. Phys. B **631**, 195 (2002) [arXiv:hep-ph/0112177].
  - [6] D. Cavalli *et al.*, “The Higgs working group: Summary report”, To appear in the proceedings of Workshop on Physics at TeV Colliders, Les Houches, France, 21 May - 1 Jun 2001, arXiv:hep-ph/0203056, and references therein.
  - [7] ATLAS Collaboration, Technical design report, Vol. 2, CERN/LHCC/99-15 (1999); CMS Collaboration, Technical Proposal, report CERN/LHCC/94-38 (1994).
  - [8] F. Wilczek, Phys. Rev. Lett. **39**, 1304 (1977); H. M. Georgi, S. L. Glashow, M. E. Machacek, and D. V. Nanopoulos, Phys. Rev. Lett. **40**, 692 (1978); J. R. Ellis, M. K. Gaillard, D. V. Nanopoulos, and C. T. Sachrajda, Phys. Lett. B **83**, 339 (1979); T. G. Rizzo, Phys. Rev. D **22**, 178 (1980) [Addendum-ibid. D **22**, 1824 (1980)].
  - [9] D. Graudenz, M. Spira, and P. M. Zerwas, Phys. Rev. Lett. **70**, 1372 (1993); M. Spira, A. Djouadi, D. Graudenz, and P. M. Zerwas, Nucl. Phys. B **453**, 17 (1995) [hep-ph/9504378].



- [10] E. L. Berger, C. W. Chiang, J. Jiang, T. M. P. Tait, and C. E. M. Wagner, arXiv:hep-ph/0205342, Phys. Rev. D (in press).
- [11] N. Kauer, T. Plehn, D. Rainwater, and D. Zeppenfeld, Phys. Lett. B **503**, 113 (2001) [arXiv:hep-ph/0012351]; T. Plehn, D. Rainwater, and D. Zeppenfeld, Phys. Rev. D **61**, 093005 (2000) [arXiv:hep-ph/9911385]; D. Rainwater and D. Zeppenfeld, JHEP **9712**, 005 (1997) [arXiv:hep-ph/9712271].
- [12] M. Carena *et al.*, “Report of the Tevatron Higgs working group,” arXiv:hep-ph/0010338.
- [13] E. L. Berger, E. Braaten, and R. D. Field, Nucl. Phys. B **239**, 52 (1984); P. Aurenche, A. Douiri, R. Baier, M. Fontannaz, and D. Schiff, Z. Phys. C **29**, 459 (1985); B. Bailey, J. F. Owens, and J. Ohnemus, Phys. Rev. D **46**, 2018 (1992); B. Bailey and J. F. Owens, Phys. Rev. D **47**, 2735 (1993); B. Bailey and D. Graudenz, Phys. Rev. D **49**, 1486 (1994) [arXiv:hep-ph/9307368]; T. Binoth, J. P. Guillet, E. Pilon, and M. Werlen, Phys. Rev. D **63**, 114016 (2001) [arXiv:hep-ph/0012191] and Eur. Phys. J. C **16**, 311 (2000) [arXiv:hep-ph/9911340].
- [14] C. Balazs, E. L. Berger, S. Mrenna, and C.-P. Yuan, Phys. Rev. D **57**, 6934 (1998) [arXiv:hep-ph/9712471]; C. Balazs and C.-P. Yuan, Phys. Rev. D **59**, 114007 (1999) [Erratum-ibid. D **63**, 059902 (1999)] [arXiv:hep-ph/9810319]; C. Balazs, P. Nadolsky, C. Schmidt, and C.-P. Yuan, Phys. Lett. B **489**, 157 (2000) [arXiv:hep-ph/9905551].
- [15] Z. Bern, L. Dixon, and C. Schmidt, arXiv:hep-ph/0206194, and references therein.
- [16] J. R. Ellis, M. K. Gaillard, and D. V. Nanopoulos, Nucl. Phys. B **106**, 292 (1976); M.A. Shifman, A. I. Vainshtein, M. B. Voloshin, and V. I. Zakharov, Sov. J. Nucl. Phys. **30**, 711 (1979) [Yad. Fiz. **30**, 1368 (1979)].
- [17] S. Dawson, Nucl. Phys. B **359**, 283 (1991); A. Djouadi, M. Spira, and P. M. Zerwas, Phys. Lett. B **264**, 440 (1991).
- [18] R. V. Harlander and W. B. Kilgore, Phys. Rev. Lett. **88**, 201801 (2002) [arXiv:hep-ph/0201206]; C. Anastasiou and K. Melnikov, arXiv:hep-ph/0207004.
- [19] R. K. Ellis, I. Hinchliffe, M. Soldate, and J. J. van der Bij, Nucl. Phys. B **297**, 221 (1988); U. Baur and E. W. Glover, Nucl. Phys. B **339**, 38 (1990); R. P. Kauffman, Phys. Rev. D **45**, 1512 (1992); S. Dawson and R. P. Kauffman, Phys. Rev. Lett. **68**, 2273 (1992); R. P. Kauffman, S. V. Desai, and D. Risal, Phys. Rev. D **55**, 4005 (1997) [Erratum-ibid. D **58**, 119901 (1998)] [arXiv:hep-ph/9610541]; V. Del Duca, W. Kilgore, C. Oleari, C. Schmidt, and D. Zeppenfeld,

- Phys. Rev. Lett. **87**, 122001 (2001) [arXiv:hep-ph/0105129]; Nucl. Phys. B **616**, 367 (2001) [arXiv:hep-ph/0108030].
- [20] D. de Florian, M. Grazzini, and Z. Kunszt, Phys. Rev. Lett. **82**, 5209 (1999) [arXiv:hep-ph/9902483].
  - [21] V. Ravindran, J. Smith, and W. L. Van Neerven, Nucl. Phys. B **634**, 247 (2002) [arXiv:hep-ph/0201114].
  - [22] C. J. Glosser and C. R. Schmidt, arXiv:hep-ph/0209248.
  - [23] J. C. Collins and D. E. Soper, Nucl. Phys. B **193**, 381 (1981) [Erratum-ibid. B **213**, 545 (1983)]; Nucl. Phys. B **197**, 446 (1982).
  - [24] J. C. Collins, D. E. Soper, and G. Sterman, Nucl. Phys. B **250**, 199 (1985).
  - [25] R. K. Ellis and S. Veseli, Nucl. Phys. B **511**, 649 (1998) [arXiv:hep-ph/9706526]; R. K. Ellis, D. A. Ross, and S. Veseli, Nucl. Phys. B **503**, 309 (1997) [arXiv:hep-ph/9704239].
  - [26] C. T. Davies and W. J. Stirling, Nucl. Phys. B **244**, 337 (1984); C. T. Davies, B. R. Webber, and W. J. Stirling, Nucl. Phys. B **256**, 413 (1985).
  - [27] P. B. Arnold and R. P. Kauffman, Nucl. Phys. B **349**, 381 (1991).
  - [28] G. A. Ladinsky and C.-P. Yuan, Phys. Rev. D **50**, 4239 (1994) [arXiv:hep-ph/9311341].
  - [29] C. Balazs, J. W. Qiu, and C.-P. Yuan, Phys. Lett. B **355**, 548 (1995) [arXiv:hep-ph/9505203].
  - [30] C. Balazs and C.-P. Yuan, Phys. Rev. D **56**, 5558 (1997) [arXiv:hep-ph/9704258].
  - [31] E. L. Berger, L. E. Gordon, and M. Klasen, Phys. Rev. D **58**, 074012 (1998) [arXiv:hep-ph/9803387].
  - [32] J. W. Qiu and X. F. Zhang, Phys. Rev. D **63**, 114011 (2001) [arXiv:hep-ph/0012348]; Phys. Rev. Lett. **86**, 2724 (2001) [arXiv:hep-ph/0012058].
  - [33] F. Landry, R. Brock, G. Ladinsky, and C.-P. Yuan, Phys. Rev. D **63**, 013004 (2001) [arXiv:hep-ph/9905391].
  - [34] X.-F. Zhang and G. Fai, arXiv:hep-ph/0205155.
  - [35] S. Catani, E. D’Emilio, and L. Trentadue, Phys. Lett. B **211**, 335 (1988).
  - [36] I. Hinchliffe and S. F. Novaes, Phys. Rev. D **38**, 3475 (1988).
  - [37] R. P. Kauffman, Phys. Rev. D **44**, 1415 (1991); R. P. Kauffman, Phys. Rev. D **45**, 1512 (1992).
  - [38] C.-P. Yuan, Phys. Lett. B **283**, 395 (1992); C. Balazs and C.-P. Yuan, Phys. Lett. B **478**, 192 (2000) [arXiv:hep-ph/0001103]; C. Balazs, J. Huston, and I. Puljak, Phys. Rev. D **63**, 014021 (2001) [arXiv:hep-ph/0002032].

- [39] D. de Florian and M. Grazzini, Phys. Rev. Lett. **85**, 4678 (2000) [arXiv:hep-ph/0008152]; Nucl. Phys. B **616**, 247 (2001) [arXiv:hep-ph/0108273].
- [40] E. L. Berger and R.-B. Meng, Phys. Rev. D **49**, 3248 (1994) [arXiv:hep-ph/9310341].
- [41] K. G. Chetyrkin, B. A. Kniehl, and M. Steinhauser, Phys. Rev. Lett. **79**, 353 (1997) [arXiv:hep-ph/9705240]; M. Kramer, E. Laenen, and M. Spira, Nucl. Phys. B **511**, 523 (1998) [arXiv:hep-ph/9611272].
- [42] A. Vogt, Phys. Lett. B **497**, 228 (2001) [arXiv:hep-ph/0010146].
- [43] S. Catani, D. de Florian, and M. Grazzini, Nucl. Phys. B **596**, 299 (2001) [arXiv:hep-ph/0008184].
- [44] G. Parisi and R. Petronzio, Nucl. Phys. B **154**, 427 (1979).
- [45] CTEQ Collaboration, H. L. Lai *et al.*, Eur. Phys. J. C **12**, 375 (2000) [arXiv:hep-ph/9903282].
- [46] W. Giele *et al.*, “The QCD/SM working group: Summary report”, in *Les Houches 2001, Physics at TeV colliders*, 275 - 426, arXiv:hep-ph/0204316.